International Journal of Pharmaceutics 640 (2023) 123005

Contents lists available at ScienceDirect

International Journal of Pharmaceutics

journal homepage: www.elsevier.com/locate/ijpharm

Formulation of antiretroviral nanocrystals and development into a microneedle delivery system for potential treatment of HIV-associated neurocognitive disorder (HAND)

Marco T.A. Abbate, Inken K. Ramöller, Akmal H. Sabri, Alejandro J. Paredes, Aaron J. Hutton, Peter E. McKenna, Ke Peng, Jessica A. Hollett, Helen O. McCarthy, Ryan F. Donnelly *

School of Pharmacy, Queen's University Belfast, 97 Lisburn Road, BT9 7BL, UK

ARTICLE INFO

Keywords:
Microneedle
Rilpivirine
Cabotegravir
HIV-associated neurocognitive disorder
HAND
Blood–brain barrier
Nanocrystal

ABSTRACT

HIV/AIDS remains a major global public health issue. While antiretroviral therapy is effective at reducing the viral load in the blood, up to 50% of those with HIV suffer from some degree of HIV-associated neurocognitive disorder, due to the presence of the blood–brain barrier restricting drugs from crossing into the central nervous system and treating the viral reservoir there. One way to circumvent this is the nose-to-brain pathway. This pathway can also be accessed *via* a facial intradermal injection. Certain parameters can increase delivery *via* this route, including using nanoparticles with a positive zeta potential and an effective diameter of 200 nm or less. Microneedle arrays offer a minimally invasive, pain-free alternative to traditional hypodermic injections. This study shows the formulation of nanocrystals of both rilpivirine (RPV) and cabotegravir, followed by incorporation into separate microneedle delivery systems for application to either side of the face. Following an *in vivo* study in rats, delivery to the brain was seen for both drugs. For RPV, a C_{max} was seen at 21 days of 619.17 ± 73.32 ng/g, above that of recognised plasma IC90 levels, and potentially therapeutically relevant levels were maintained for 28 days. For CAB, a C_{max} was seen at 28 days of 478.31 ± 320.86 ng/g, and while below recognised 4IC90 levels, does indicate that therapeutically relevant levels could be achieved by manipulating final microaaray patch size in humans.

1. Introduction

Human immunodeficiency virus (HIV), which can develop further to acquired immunodeficiency syndrome (AIDS), continues to be one of the major global health problems faced today. If not managed appropriately. In 2020, there were 37.7 million people living with HIV (PLWH), with 28.2 million of these people accessing antiretroviral therapy (ART) (Joint United Nations Programme on HIV/AIDS (UNAIDS), 2021). In recent times, antiretroviral therapy (ART) has become very effective. One of the main contributions to this success is combination therapy, where different drug classes acting at different stages of the HIV replication cycle can be administered in combination to inhibit replication and decrease the likelihood of resistance. One such combination is that of rilpivirine (RPV) and cabotegravir (CAB) (Moffatt et al., 2022; Ramöller et al., 2022; Sanford, 2012). RPV is a second-generation non-nucleoside reverse transcriptase inhibitor (NNRTI), and is a white crystalline powder which is practically insoluble in water with a log P > 4.16. CAB is an integrase inhibitor, which is also practically insoluble in water at pH of < 10, and has a log P of 0.16. These can be given together as separate tablets in a once-daily oral dosing regimen, or as separate long-acting injections in a monthly or two-monthly intramuscular (IM) injection (European Medicines Agency, 2020a, 2020b, 2011). However,

Abbreviations: %DTE, drug targeting efficiency; %DTP, direct transport percentage; ACN, acetonitrile; AIDS, acquired immunodeficiency syndrome; ART, antiretroviral therapy; ARV, antiretrovirals; ATR-FTIR, attenuated total reflectance Fourier-transformed infrared spectroscopy; AUC, area under the curve; BBB, blood–brain barrier; CAB, cabotegravir; CNS, central nervous system; DLS, dynamic light scattering; ESI, electrospray ionisation; HAND, HIV-associated neurocognitive disorder; HIV, human immunodeficiency virus; HPLC, high-performance liquid chromatography; LLOQ, lower limit of quantification; LOD, limit of detection; MAP, microarray patch; MN, microneedle; MS, mass spectrometry; NC, nanocrystal; NNRTI, non-nucleoside reverse transcriptase inhibitor; PALS, phase analysis light scattering; PBS, phosphate buffered saline; PDI, polydispersity index; PVA, poly(vinyl alcohol); PVP, poly(vinyl pyrrolidone); RPV, rilpivirine; TFA, trifluoroacetic acid; UV, ultraviolet; WBM, wet bead milling; ZP, Zeta potential.

* Corresponding author at: School of Pharmacy, Queen's University Belfast, Medical Biology Centre, 97 Lisburn Road, Belfast BT9 7BL, Ireland.

https://doi.org/10.1016/j.ijpharm.2023.123005
Received 13 March 2023; Received in revised form 26 April 2023; Accepted 27 April 2023
Available online 2 May 2023

these IM injections are not self-administered, and generate sharps and potentially infected waste. Also, while they can maintain virological suppression in the blood, there are many other reservoirs which they are unable to treat as effectively, such as the brain and the lymph.

Due to the success of ART, PLWH are now living longer, and as a result are experiencing more co-morbidities, including HIV-associated neurocognitive disorders (HAND) (Edagwa et al., 2014; Ntshangase et al., 2019; Scherrer et al., 2022; Zayyad and Spudich, 2015). Up to 50% of all those infected with HIV will develop some degree of HAND, occurring as a result of a reservoir of HIV in the brain, and due to the presence of blood–brain barrier (BBB), is protected from ART (Edagwa et al., 2014; McArthur, 2004). The brain is, however, not the only reservoir of the virus found in the body, with the lymph being a well-recognised sanctuary of HIV (Banga et al., 2021; Scholz and Kashuba, 2021). One method of bypassing the BBB is *via* the nose-to-brain pathway, where formulations are administered intranasally, and transported passively *via* the olfactory and trigeminal nerve pathways directly to the brain (Formica et al., 2022; Mistry et al., 2009). It is hypothesised that it is the trigeminal nerve pathway, outlined in Fig. 1, that provides the most likely pathway for antivirals, particularly those with low molecular weight, to reach the brain. To enhance the delivery *via* this route, nanocrystals (NCs) are often used. NCs are one subset of nanoparticles that are essentially pure, nanometre-sized drug crystals, and have numerous advantages as a result, including a high-drug loading and lack of excipient related toxicity (Formica et al., 2022; McGuckin et al., 2022). Recent reviews highlight the advantages of NCs, and their use in delivery *via* the nose-to-brain pathway (Formica et al., 2022; McGuckin et al., 2022). While formulations with a wide range of particle characteristics have been successfully delivered, delivery appears to be particularly enhanced when NCs are formulated to have a size of<200 nm and a positive Zeta potential (ZP) (Agrawal et al., 2018; Formica et al., 2022; Mistry et al., 2009; Selvaraj et al., 2018).

It has also been shown that using a facial intradermal injection, formulations can be delivered into the skin and passively transported to the brain *via* these same neural pathways, without the drug being administered intranasally (Yang et al., 2022; Yu et al., 2017). This was demonstrated using a hypodermic needle, which carries a separate set of concerns, such as trypanophobia, associated pain, the medical personnel to administer the formulation, and the generation of both sharps and potentially infectious waste (Donnelly et al., 2012; Tuan-Mahmood et al., 2013). One way to circumvent these issues is using microneedle (MN) technology and microarray patches (MAP).

MN technology involves using minimally invasive needles of a micron scale, which when inserted into the skin are pain-free, and potentially avoid the associated needle phobia (Alkilani et al., 2015; Donnelly et al., 2012; Tuan-Mahmood et al., 2013). There are five main categories of MN, namely solid, coated, hydrogel-forming, hollow and dissolving (Alkilani et al., 2015; Tuan-Mahmood et al., 2013). Hollow MNs are used as an alternative method of performing intradermal injections, with the MNs sub-micron length offering greater control over injection depth and therefore ensuring an intradermal administration, while avoiding associated needle phobia and pain. Dissolving MNs incorporate the payload with hydrophilic polymers such that when inserted into the skin, the MNs dissolve in the interstitial fluid available, depositing the loaded drug intradermally. Dissolving MAPs are, therefore, potentially ideal candidates for self-administration and are self-disabling, with the MNs being unable to be reinserted as they have dissolved.

To date, there have not been any reports of a facial MN application being used for targeted brain delivery. The overall aim of the study was to combine MN technology, NCs and the neural transport routes to deliver RPV and CAB directly to the brain, for the potential treatment of HAND. To test this hypothesis, an *in vivo* study is needed.

2. Materials and methods

2.1. Materials

PVA 9–10 kDa, D-α-Tocopherol polyethylene glycol 1000 succinate (TPGS), trifluoroacetic acid (TFA) (suitable for HPLC, ≥ 99.0%), acetonitrile (ACN) (suitable for HPLC, gradient grade, ≥ 99.9%), trehalose, mannitol, chitosan (medium molecular weight), methyl cellulose, phosphate buffered saline (PBS) pH 7.2–7.6 and acetic acid (glacial, ReagentPlus®, ≥ 99.0%) were purchased from Sigma-Aldrich (St. Louis, MO, USA). PVP 58 kDa and PVP 360 kDa, marketed as Plasdone™ k29/32 and Plasdone™ k90 respectively, were obtained from Ashland (Wilmington, DE, USA). RPV was provided by Janssen Pharmceutica (Beerse, Belgium). CAB was provided by ViiV Healthcare Ltd. (Brentford, UK). Poly(lactic acid) (PLA) was purchased from Ultimaker (Utrecht, Netherlands). Nanosoft™ hollow microneedle arrays were purchased from Fillmed (Paris, France). For the neonatal porcine skin that was used *ex vivo*, stillborn piglets were obtained from a local farm immediately after birth and excised full-thickness skin was stored at −20 °C until further use.

2.2. Analytical methods

2.2.1. Analytical method to be used in vitro and ex vivo

All *in vitro* analysis was carried out using reverse-phase HPLC coupled with a UV detector on an Agilent 1220 Infinity LC system, with an Apex Scientific Inertsil ODS-3 column with a 5 μm particle size, an internal diameter of 4.6 mm and 250 mm column length. The column

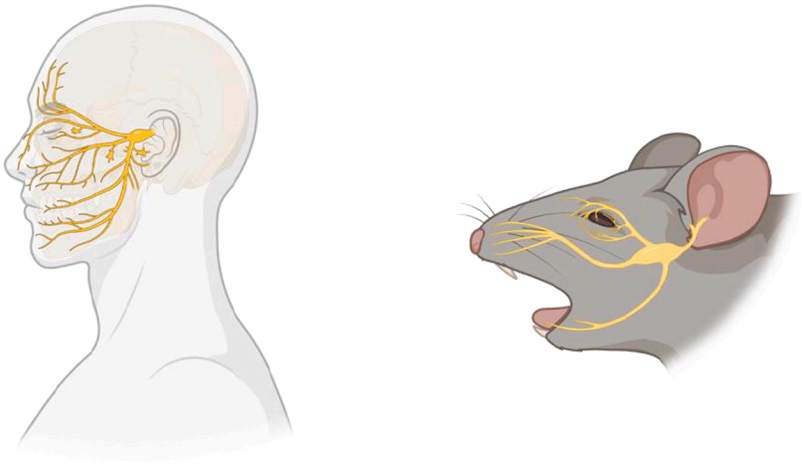

Fig. 1. A schematic of the trigeminal innervation in a human and in a rodent. Produced using BioRender.com (2022).

temperature was maintained at 40 °C with an isocratic mobile phase consisting of ACN:TFA 0.1% in water (81:19) and a flow rate of 0.3 ml/min. The absorbance was set at 257 nm, the injection volume set to 30 µl and run time was set to 12 min.

2.2.2. Analytical methods to be used in vivo

For simultaneous detection, separation and quantification of analytes from *in vivo* samples, a more sensitive detector was needed. Reverse-phase HPLC coupled with a single quadrupole MS detector was used in the form of an Agilent 1260 Infinity II system (Ramöller et al., 2022). The column used was an Apex Scientific Inertsil ODS-3 column with a 5 µm particle size, an internal diameter of 4.6 mm and 250 mm column length. This was preceded with a Phenomenex® SecurityGuard™ guard cartridge of matching chemistry. The column temperature was maintained at 40 °C with an isocratic mobile phase consisting of ACN:TFA 0.1% in water (81:19) and a flow rate of 0.3 ml/min. The injection volume was set at 15 µl and run time was set to 13 min. Samples were ionised using electrospray ionisation (ESI) and detected in positive ion mode at the corresponding $(M + H)^+$ peaks for lymph and plasma, while for the brain tissue samples additional $(M + Na)^+$, $(M + Cl)^+$, $(M + K)^+$ and $(M-H)^-$ signals for both RPV and CAB were to be measured, due to the tendencies of adduct ions to form in brain tissue (Matsumoto et al., 2021; Otoki et al., 2015; Ramöller et al., 2022).

2.3. Measurement of particle size, PDI and ZP

Using a NanoBrook Omni (Brookhaven Instruments, Holtsville, NY, USA) particle size and PDI analysis was conducted using dynamic light scattering (DLS), and ZP analysis was conducted using phase analysis light scattering (PALS). Particle size is expressed as the effective diameter. All measurements performed in triplicate and displayed as means ± standard deviation (S.D.).

2.4. Preparation of NCs of RPV and CAB

Wet bead milling (WBM) is a common 'top-down' method used in the production of NCs. It is an industrially accepted process with low inter-batch variability and a lack of organic solvents used (McGuckin et al., 2022; Romero et al., 2016a). While WBM can be performed on an industrial scale, it has been shown that it can be performed on a much smaller benchtop scale, without the use of planetary mill equipment (Romero et al., 2016a, 2016b). A modified version of the method described by Romero et al. (2016) was used to formulate the RPV and CAB NCs. To formulate both sets of NCs, the vessel used was a 7 ml glass vial and the energy was provided to the system using a magnetic stir plate set at 1250 rpm and two 15 × 8 mm magnetic stir bars. The milling media used were yttrium stabilised zirconium oxide beads of 0.1–0.2 mm in diameter, which encompassed approximately 20% of the total volume of space available in the vial. The surfactant solution used was 5 ml of an aqueous mix of chitosan 0.05% w/w, which had first been dissolved in acetic acid and diluted appropriately, and TPGS 1.02% w/w. For the RPV NCs, 440 mg of drug was added to each batch, while for the CAB NCs the drug added amounted to 400 mg. These were milled for 20 h, before the resultant nanosuspensions were recovered through a nylon 200-mesh sieve and the beads rinsed with a known quantity (3 ml) of water to ensure a more efficient recovery of the NCs. This yielded seven full 1 ml portions of each NC formulation. The resultant NCs, both RPV and CAB, were then analysed using DLS and PALS. Separately, these nanosuspensions were left for a period of 6 months in various ambient conditions to determine their particle size stability over time.

2.5. Lyophilisation of RPV and CAB NCs

To both concentrate the samples and increase the long term stability of the samples, the nanosuspensions can be converted to a solid form, commonly *via* lyophilisation and often involving cryoprotectants in the form of common excipients such as sugars and hydrophilic polymers (Bozdag et al., 2005; Gol et al., 2018; Kumar et al., 2014). To assess how different cryoprotectants were able to resist changes in particle characteristics during the lyophilisation process, different excipients were trialled with the RPV NC as in Table 1. Recovered 1 ml batches of RPV NCs were mixed with the excipients and lyophilised according to the protocol as previously described (Donnelly et al., 2014). Following the rationalisation of excipient choice with the RPV NCs, the most promising was also used with the CAB NC. Following lyophilisation, particle analysis was performed using DLS and PALS, with all measurements performed in triplicate. Results for each excipient are displayed as a ratio of the particle size post- and pre-lyophilisation (Gol et al., 2018).

The samples were pre-frozen at −80 °C, and the lyophilisation protocol as follows: Primary drying: 90 mins at a shelf temperature of −40 °C, 90 mins at a shelf temperature of −30 °C, 90 mins at a shelf temperature of −20 °C, 530 mins at a shelf temperature of −10 °C and 90 mins at a shelf temperature of 0–10 °C. The secondary drying phase took place over 660 mins at a shelf temperature of 25 °C and a vacuum pressure of 50 mTorr (Donnelly et al., 2014; Rojekar et al., 2021; Volpe-Zanutto et al., 2021).

2.6. Physical characterisation of formulated NC

To determine the drug content of the lyophilised NCs, a known amount of formulation was taken from several distinct batches of each formulation and uniformly dispersed in 10 ml of water with the use of a vortex mixer. Once redispersed, an aliquot of 100 µl was taken from each sample and vortexed thoroughly with 1900 µl of ACN to solubilise the drug and precipitate polymers. Samples were then centrifuged at 14,000 *g* for 10 min to sediment any impurities and the resultant supernatant analysed using HPLC-UV as in 2.2.1.

To establish any possible interactions in the NC formulations, attenuated total reflectance Fourier transformed infrared analysis was performed using an Accutrac FT/IR-4100 series infrared spectrophotometer (Perkin Elmer, Waltham, MA, USA). Scans of each lyophilised NC formulation as well as individual components and excipients were taken, as well as physical mixtures of the components. In total, 32 scans were taken for each sample between 4000 and 600 cm^{-1} with a 4 cm^{-1} resolution.

2.7. Ex vivo delivery using MN array

2.7.1. Extraction of analytes from porcine skin

To extract analytes from pig skin in *ex vivo* studies, skin was roughly chopped on a clean glass slide with a scalpel and placed in a 2 ml Eppendorf tube with 2 stainless steel metal beads and 500 µl of deionised water. Tubes were then placed in a TissueLyser LT (Qiagen Ltd., Manchester, UK) and homogenised at 50 Hz for 10 min. Following this, 1 ml of ACN was added and a further homogenisation at 50 Hz for 20 min was commenced. The tubes were then placed under sonication for 30 min, followed by centrifugation at 14,000 *g* for 10 min at 4 °C. A 100 ml aliquot of supernatant was taken and diluted appropriately before analysed using HPLC-UV (Moffatt et al., 2022; Rojekar et al., 2021).

Table 1
The different cryoprotectants used for the lyophilisation of rilpivirine (RPV) and cabotegravir (CAB) nanocrystals (NCs). The poly(vinyl alcohol) (PVA)/poly (vinyl puyrrolidone) (PVP) mixture was an aqueous solution of PVA 9–10 kDa and PVP 58 kDa respectively.

Formulation	Cryoprotectanr	Quantity
RPV NCs	Mannitol	5% w/v
RPV NCs	Trehalose	5% w/v
RPV NCs	Trehalose	10% w/v
RPV NCs	PVA/PVP 2%/2%	1:1 vol ratio
CAB NCs	PVA/PVP 2%/2%	1:1 vol ratio

2.7.2. Determination of extraction efficiency of analytes from porcine skin

To ensure results are accurate from *ex vivo* studies, it must be known if RPV and CAB can successfully be extracted from porcine skin, and to what extent recovery of the analytes can be made. To determine this, 1 mg of RPV in the form of reconstituted NC and 1 mg of CAB in the form of reconstituted NC were added to separate 2 ml Eppendorfs containing 1 cm^2 of prepared excised full thickness neonatal porcine skin that had been shaved and chopped roughly. These were then incubated at 37 °C for 24 h. Control samples with no skin and only formulation were incubated in the same conditions (n = 6) (Rojekar et al., 2021). Following this, drug was extracted and analysed using HPLC-UV, and extraction efficiency could be calculated.

2.7.3. Creation of an in vivo model for mystacial pad intradermal injection

With a long-term view towards use in human patients, it was envisioned that a MAP containing RPV NCs could be applied to one side of a patients face, and a MAP containing CAB NC could be applied to the other side of a patients face before they go to sleep, and the undissolved baseplate could be removed when they were to wake. While ultimately these MAPs are hypothesised for use in humans, *in vivo* studies in animal models can be of great benefit to assess the effectiveness of delivery system and the distribution of the drug once it is in the body. To date, there have been no studies showing the application of a MAP to the face with the intention of delivering drugs intradermally and *via* neural pathways to the brain. However, this pathway has been targeted using injections with traditional hypodermic needles (Yang et al., 2022; Yu et al., 2017). As this pathway has been shown to be accessible in rats, this was the *in vivo* model chosen for this study. With a MAP, this area for administration is not so straightforward. This area of application is curved, and consistent MN insertion throughout the full array would be needed. Also, the whiskers present in this area are essential for the rats feeling and spatial awareness, and removing these prior to MAP insertion could be described as unethical, and so any MAP applied to this area must be able to penetrate through the whiskers and fur present (Diamond and Arabzadeh, 2013). Not only this, but the area available in the rat is relatively smaller than those in humans would be, limiting the size of the array that is available for use. In other MN based studies, the MAPs are often secured in place for the initial 24 h period (Moffatt et al., 2022; Tekko et al., 2022; Volpe-Zanutto et al., 2022). In this case, securing the MAPs to the application site could result in difficulties eating, drinking and even breathing for the rats, and so this was ruled out as an option, ethically. As a result the MAP can only be applied to the animals while they are anaesthetised, and for simple procedures under general anaesthesia, under the establishment license available this was restricted to a period of only 15 min. This 15 min included the time to initiate anaesthesia and for complete recovery. All these factors contribute to a challenging *in vivo* study, which must involve careful rationalisation of the MN delivery system.

While the time available can be simulated easily *ex vivo*, the curvature of the rat's face and area available cannot be as readily modelled. To study how these factors may have an effect, a to-scale rat head was created, atop which excised porcine skin could be overlaid to simulate insertion *in vivo*. First, a 3D scan was taken using the Qlone application on an iPad Pro (Apple Inc. CA, USA) of a rat which had been placed on a calibration chart, enabling a 1:1 scale model to be printed in PLA using the Ultimaker 3, as shown in Fig. 2. Once the model rat head was printed, skin could be overlaid and the MNs inserted to offer an *in vivo* model.

2.8. Formulation of RPV and CAB NCs into MN arrays for use in vivo

Due to the short application time available *in vivo*, the decision was

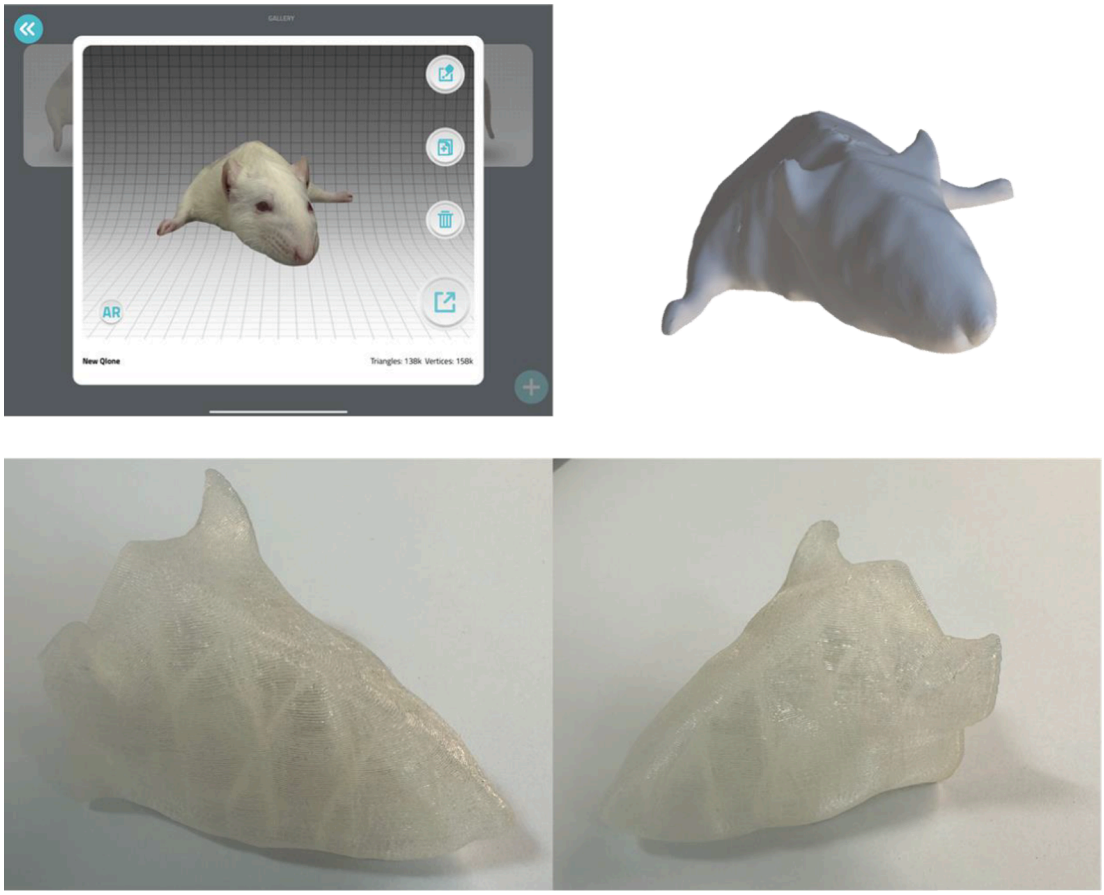

Fig. 2. The 3D scans, computer model, and final 3D-printed poly(lactic acid) model rat head.

made to focus on delivering the NC using a hollow MN system, which removes the obstacle of dissolution time of the MNs associated with dissolving MAPs. In this instance, 100 mg of either lyophilised NC formulation was reconstituted with 1 ml of water using the Speed-Mixer™ and drawn into 1 ml Luer lock syringes. Then, a Nanosoft™ hollow MN array was attached. Each Nanosoft™ array contained 3 individual MNs of 600 μm length, with the bore of the MNs being off centred to reduce risk of blockage. Intradermal injection volumes are generally limited to the intradermal space available, and this volume is generally capped at 50 – 100 μl per site. The model rat head was used for deposition studies, where the arrays were inserted into the skin which had been overlaid on the to-scale model, as in Fig. 3, and 50 μl of formulation was injected through the Nanosoft™ array, into the skin. The skin was then processed as described in 2.11.1 and analysed *via* HPLC-UV to determine the quantity of drug delivered to the skin (n = 6 for each formulation).

2.9. Delivery of RPV and CAB to the mystacial pads of Sprague-Dawley rats

2.9.1. Ethical approval

The Ethical Committee of the Queen's University Belfast Biological Services Unit reviewed the study design and provided approval for the *in vivo* study involving facial intradermal delivery of RPV and CAB NCs. The study was carried out under Project License No. 2903 and Personal License numbers 2154, 2059, 2127, 2058 and 2056. All procedures were carried out according to policy of the Federation of European Laboratory Animal Science Associations and the European Convention for the Protection of vertebrate animals used for experimental and other scientific purposes with implementation of the principles of the 3Rs (replacement, reduction and refinement).

All rats used in the study were female Sprague-Dawley rats which were 9–11 weeks old (273.1 ± 28.3 g) at study commencement and had acclimatised to their new environment for at least 7 days prior to study commencement. There were two cohorts in the study, the MN treatment group and the oral control group, with four rats per timepoint per cohort. At predetermined timepoints following drug administration, rats were culled *via* rising CO_2 concentration, followed by cervical dislocation.

2.9.2. Preparation of oral gavage for control arm of study

In the oral control group each rat was to receive, *via* an oral gavage, 1 ml of a suspension containing both RPV (2.5 mg/ml) and CAB (2.5 mg/ml). The suspensions were aqueous in nature and consisted of a base of methylcellulose 0.5% w/v. Briefly, suspensions of either RPV or CAB at 5 mg/ml were formulated by weighing an appropriate amount of drug into a glazed mortar and incorporating small portions of methylcellulose 0.5% w/v until a smooth paste was formed. This was then transferred to a glass vial and made up to the required volume with further methylcellulose 0.5% w/v. Immediately before administration, the RPV and CAB 5 mg/ml suspensions were mixed together in a 1:1 ratio to form a combined 2.5 mg/ml suspension. These suspensions were prepared no longer than six hours before intended use and combined immediately before administration.

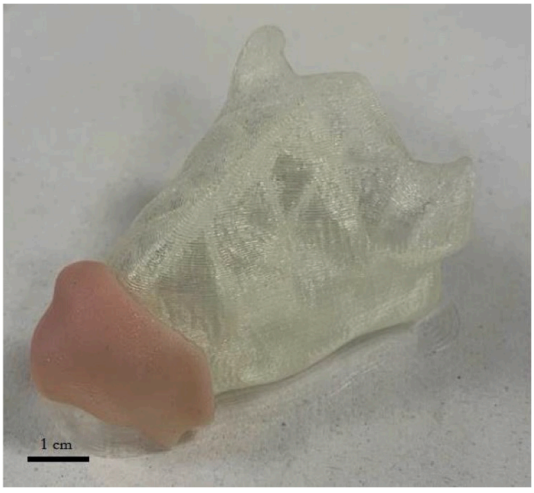

Fig. 3. Experimental set-up used for the *ex vivo* delivery into porcine skin.

2.9.3. MN mediated delivery of RPV and CAB to the mystacial pads

In the treatment arm of the study, advice was sought from the Named Veterinary Surgeon at the establishment, to ascertain if there were any concerns regarding the procedure. Two main points were raised which included the potential for pain to be caused in the rats due to the highly innervated area of administration, and the volume of intended administration. It was deemed necessary to provide prophylactic pain relief to the animals. This was in the form of a subcutaneous injection of buprenorphine 0.05 mg/kg aqueous solution one hour before MN administration of RPV and CAB NC, and a second 0.05 mg/kg dose six hours post-MN administration. For the administration volume, the Named Veterinary Surgeon advised a more cautious approach, with a volume of 100 μl/kg deemed appropriate. As during experimental planning rats were estimated to weigh approximately 250 g, injection volume was set at 25 μl. The study was in place for 28 days following a single dose of RPV and CAB to coincide with the marketed IM dosing schedule, and drug levels in the plasma, lymph and brain were all analysed.

Due to the presence of whiskers and fur on the mystacial pad of the rat, the most suitable area to administer the MN-mediated intradermal injection was to the mystacial pad with the rats in a supine position, as in Fig. 4. Rats were first sedated by gaseous anaesthesia by using 2–4% isoflurane in oxygen, and placed in the supine position. The skin on the mystacial pad was lightly pulled down so the skin was taught, the area swabbed with 70% v/v ethanol and the Nanosoft™ array, attached to a loaded syringe, was inserted and 25 μl delivered. RPV NCs were administered to the rats right-sided mystacial pad, with CAB NCs delivered to the rats left-sided mystacial pad. For each administration, a new MN array was used.

2.9.4. Collection of tissue from Sprague-Dawley rats

At predetermined timepoints (namely 1 day, 3 day, 7 day, 14 day, 21 day and 28 day) rats were Schedule 1 culled *via* rising CO_2 concentration followed by cervical dislocation. Blood was collected into heparinised tubes following cardiac puncture, which was then centrifuged at 4000 *g* and 4 °C for 10 min to separate the plasma, from which an aliquot of 100 μl was placed in an Eppendorf tube and frozen at −20 °C until further use. Following dissection of the rats, axillary and inguinal lymph nodes were collected and rinsed in PBS to remove contaminants such as blood and fur before being frozen at −20 °C until further use. Brains were removed from the rats intact, rinsed in PBS to remove contaminants such as blood and bone fragments, snap frozen in liquid nitrogen and stored at −80 °C until further use.

2.9.5. Extraction of analytes from plasma, lymph and brain tissue

To extract analytes from *in vivo* samples, 900 μl of ACN was added to each plasma sample. These were vortexed for 15 min to both precipitate proteins and to extract the drugs. Samples were then centrifuged at 14,000 *g* and 4 °C for 10 min, when the supernatant was then removed and placed into a glass culture tube. These were then placed into the Zymark TurboVap® LV Evaporator Workstation (McKinley Scientific, Sparta, NJ, USA) set at 35 °C and under a stream of nitrogen at 5 psi for 30 min. The residue was reconstituted in 100 μl of mobile phase, ACN: TFA 0.1% in water (81:19), which was vortexed for 30 s and transferred to a 0.5 ml Eppendorf tube. This was centrifuged again at 14,000 *g* and 4 °C for 10 min to sediment out any impurities, and 80 μl of the resultant

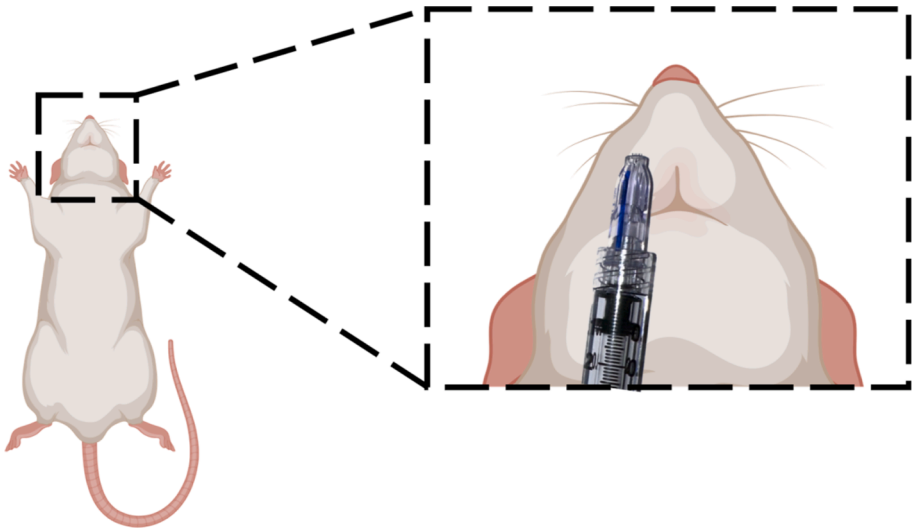

Fig. 4. The orientation of the rat for administration of nanocrystals *via* the Nanosoft™ hollow microneedle array. In this case, it would be the rilpivirine being administered, as the delivery is being performed in the rats right-sided mystacial pad. Produced using BioRender.com (2022).

supernatant was taken to be analysed using HPLC-MS as described in 2.2.2.

To extract analytes from lymph *in vivo* samples, they were first homogenised in a TissueLyser with 50 µl of water and two 5 mm stainless steel beads at 50 Hz for 10 min, followed by addition of 900 µl of ACN and a further homogenisation step at 50 Hz for 20 min was commenced to extract the drugs. Samples were then centrifuged at 14,000 *g* and 4 °C for 10 min, when the supernatant was then removed and placed into a glass culture tube. These tubes were then placed into the Zymark TurboVap® LV Evaporator Workstation set at 35 °C and under a stream of nitrogen at 5 psi for 30 min. The residue was reconstituted in 100 µl of mobile phase, ACN:TFA 0.1% in water (81:19), which was vortexed for 30 sec and transferred to a 0.5 ml Eppendorf tube. This was centrifuged again at 14,000 *g* and 4 °C for 10 min to sediment out any impurities, and 80 µl supernatant was taken to be analysed using HPLC-MS as described in 2.2.2.

To extract analytes from brain standards *in vivo* samples, individual brains were first homogenised on a clean glass tile with a scalpel, before 100 mg samples were taken from each brain homogenate and placed in an Eppendorf tube. Following this, 50 µl of TFA 1% was added to each sample and they were sonicated for 15 min. Next, two stainless steel beads of 5 mm diameter were added to each tube and samples were then placed in the TissueLyser at 50 Hz for 10 min. To each sample, 900 µl of cold (-20 °C) ACN was then added and these were then placed back into the TissueLyser at 50 Hz for 20 min to extract the drugs. Samples were then centrifuged at 14,000 *g* and 4 °C for 10 min, when the supernatant was then removed and placed into glass culture tubes. These tubes were then placed into the Zymark TurboVap® LV Evaporator Workstation set at 35 °C and under a stream of nitrogen at 5 psi for 30 min. The residue was reconstituted in 200 µl of mobile phase, ACN:TFA 0.1% in water (81:19), which was vortexed for 30 s and 100 µl of which was then transferred to a 0.5 ml Eppendorf tube. This was centrifuged again at 14,000 *g* and 4 °C for 10 min to sediment out any impurities, and 80 µl supernatant was taken to be analysed *via* HPLC-MS as in 2.2.2.

The concentrations of these analytes in plasma, lymph tissue and brain tissue could then be plotted over the course of the 28 day study. Lymph tissue was to be analysed as a secondary-site, with the aim that if the NCs were engulfed by phagocytes at the application site, they could be transported to the lymph for eradication of the viral reservoir there.

2.9.6. Calculation of biodistribution parameters

Mean maximum concentrations (C_{max}) were determined from the raw data, as well as the timepoints of these (t_{max}). While specifically looking at brain delivery in this instance, plasma and lymph levels were also analysed. More specifically looking at the brain, as this was the primary target of the study, the delivery can be assessed by calculating the drug targeting efficiency percentage (%DTE) and the direct transport percentage (%DTP), commonly used to assess efficiency of delivery to the brain *via* the nose-to-brain pathway (Mahajan et al., 2014; Masjedi et al., 2020; Muntimadugu et al., 2016; Noorulla et al., 2022). Due to the limited timepoints in the biodistribution study, concentration levels were used instead of area under the curve (AUC) values at each timepoint.

The %DTE measures the relative exposure of the brain to the drug following MN administration when compared to systemic oral delivery and was calculated at each time point using Eq. (1), where the matrix is determined with 'B' for brain or 'P' for plasma. Values can range from -∞ to +∞ and values higher than 100% indicate more efficient delivery *via* the MN route (Muntimadugu et al., 2016).

$$\%DTE = \frac{C_{MN-B}/C_{MN-P}}{C_{OG-B}/C_{OG-P}} \quad (1)$$

The %DTP measures the percentage of the dose that is estimated to be transported to the brain directly following MN administration when compared to systemic oral delivery and is calculated using Eq. (2). Values can range from -∞ to + 100%, with any value above 0 indicating an effective brain targeting (Muntimadugu et al., 2016).

$$\%DTP = \frac{C_{MN-B} - \left(\frac{C_{OG-B}}{C_{OG-P}} \times C_{MN-P}\right)}{C_{MN-B}} \quad (2)$$

2.10. Statistical analysis

Data is presented as means ± S.D, unless otherwise stated in the figure legend. All statistical analysis was performed using GraphPad Prism (version 9, GraphPad Inc., San Diego, CA, USA) and $p < 0.05$ denotes statistical significance. Statistical tests performed were *t*-tests. No AUC analysis was undertaken due to variation in results. Plasma levels for RPV of above the IC90 of 12 ng/ml denoted therapeutic relevance, with CAB levels above the 4IC90 of 664 ng/ml are denoted as therapeutically relevant (Landovitz et al., 2020; Patel et al., 2019; Tekko et al., 2022; Whitfield et al., 2016; Williams et al., 2015). These were translated to 12 ng/g and 664 ng/g of tissue, respectively. This approach is commonly used when it is unknown if tissue binding is similar to protein binding (Labarthe et al., 2022). Any values obtained from analytical methods that were detectable, but below the lower limit of

quantification (LLOQ), were treated as having a value equal to the limit of detection (LOD) for that matrix.

3. Results and discussion

3.1. Analytical method validation

A simple HPLC-UV method was validated for use *in vitro* according to ICH guidelines. This HPLC-UV method had a linear range of 0 – 25 μg/ml, with an LOD of 0.11 μg/ml and an LLOQ of 0.33 μg/ml for RPV, with an LOD of 0.50 μg/ml and an LLOQ of 1.52 μg/ml for CAB. At high (25 μg/ml), medium (10 μg/ml) and low (5 μg/ml) concentration points of the validated range, the method was assessed for accuracy and precision, both of which came within recommended guidelines (95–105% recovery for accuracy, <5% coefficient of variance (CV) for precision) for these parameters for both drugs (European Medicines Agency, 1995). This method was then adapted for use *in vivo* and validated in plasma and lymph samples as previously shown by Ramöller et al. (2022). For the brain samples, and as shown for the lymph samples, a partial validation was conducted with the validated range split into two separate calibration curves, from 50 to 750 ng/ml and from 750 to 10,000 ng/ml. For RPV, the LOD was 59.34 ng/ml with an LLOQ of 179.32 ng/ml, while for CAB the LOD was 61.81 ng/ml and the LLOQ was found to be 187.32 ng/ml. For bioanalytical method validation, calculations were performed at high, medium and low concentration points for each calibration curve. The ICH recommends a limit of ± 15% for recovery, which was found to be true in this case, indicating a highly accurate method (European Medicines Agency, 2022). However, while all CAB precision was found to be within the ICH recommended 15% CV, RPV values fell outside these recommended limits. It must be stressed that the ICH guideline M10 on bioanalytical method validation is strictly only guidance and recommendations, and this should not present an issue for proof-of-concept exploratory science, particularly due to the well-recognised challenging nature of quantifying analytes in brain tissue. If this study was to be taken further, or presented as pre-clinical data, this method may need revalidated. Other published articles dealing with brain quantification often propose a more lenient 20% CV, and even so published data may still lie outside these limits (De Angelis et al., 2020; Munyeza et al., 2016; Reiter and Stimpfl, 2015).

Calculation of the extraction efficiency of both RPV and CAB from neonatal porcine skin was also conducted. For RPV, the extraction efficiency was calculated to be 96.58% while CAB was calculated to be 96.23%. This high extraction efficiency can be attributed to the drugs high solubilities in ACN, and these values can be factored into *ex vivo* studies to determine accurately the quantity of drug delivered to the skin.

3.2. Formulation of NCs of RPV and CAB

NCs of RPV and CAB were produced *via* the top-down method of WBM for 20 h, and particle characteristics are shown in Table 2. These formulations are within the desired limits for both particle size and ZP. With NCs, a decrease in particle size can result in an increase in solubility due to an increase in surface area-to-volume ratio. As the aim of this study was to form a depot of NCs at the injection site, decreasing the particle size further may have a negative effect on the residence time of the NCs at the injection site, due to this potentially increased solubility. Futhermore, decreasing the particle size further occurs at the expense of longer milling times, and as a result an increased manufacturing cost. As a result, approximately 200 nm was chosen as the target size. Both formulations also have a narrow PDI, indicating a uniform distribution of particles (Fig. 5a) which reduces the risk of Ostwald's ripening over time (Li et al., 2020; Pawar et al., 2014; Verma et al., 2011). This narrow PDI therefore indicates a good stability profile for the formulation, and as seen in Fig. 5b after 6 months both formulations were seen to remain<200 nm in mean particle size.

Table 2
The particle characteristics of formulated rilpivirine (RPV) and cabotegravir (CAB) nanocrystals. (means ± S.D., n = 3).

Formulation	Eff. Diameter (nm)	PDI	ZP (mV)
RPV	163.13 ± 5.46	0.109 ± 0.006	16.87 ± 0.53
CAB	194.79 ± 2.70	0.129 ± 0.037	17.29 ± 0.26

The ZP measurement is positive for both formulations, as desired, and is largely due to the presence of chitosan in the milling chamber. Chitosan is known to impart a positive ZP on nanosystems, and unlike other cationic surfactants considered for use, is well tolerated and non-toxic to humans (Dalpiaz and Pavan, 2018; Hanafy et al., 2015; Kurakula et al., 2015; Mistry et al., 2009). In combination with this, the TPGS acts as a surfactant to stabilise the system. It has good acid stability, necessary when combining with chitosan which is only soluble in acidic conditions. Additionally, TPGS may inhibit PGP efflux pumps, allowing for a longer residence time of the formulation in the desired site (Collnot et al., 2010; Guo et al., 2013; Liu et al., 2018; Yang et al., 2018).

These formulations were manufactured to the characteristics desired, and by viewing the particle size reduction over time in Fig. 5c it is clear that milling time could be reduced, which when considering a translation to industry could result in decreased formulation costs and time. The long-term stability of the size of the NCs is beneficial too as it demonstrates that there is a reduced urgency to lyophilise the NCs immediately after milling.

3.3. Lyophilisation of NCs

The effect of the lyophilisation process on particle size was assessed, including with the use of cryoprotectants. The ability of different cryoprotectants to resist changes in particle size is seen in Table 3. Some readouts on the particle sizer resulted in errors post-lyophilisation due to the inability of the cryoprotectant to resist changes in particle size to such an extent that the NCs were not able to be analysed by the DLS.

Lyophilisation with sugars commonly employed as cryoprotectants, namely trehalose, mannitol and sorbitol, were trialled, however could not resist changes in particle size to the desired degree, and it was a mixture of PVA/PVP that was shown to be the most effective. The NC with this PVA/PVP mixture resisted changes in particle growth so that there was no significant difference before and after lyophilisation ($p > 0.05$ for both RPV and CAB). As these are the polymers that are commonly used in the formulation of dissolving MAPs, this negates any possible compatibility issues in comparison with the sugars that were trialled, which have tendencies to cause needles in the dissolving arrays to become brittle with poor insertion characteristics. These polymers used are also biocompatible, and so this is the formulation that was carried forward, not only for their cryoprotectant ability, but the compatibility benefits (Singh et al., 2016; Tekko et al., 2020).

3.4. Physical characterisation of NCs

From using HPLC-UV to determine recovery, the drug content of lyophilised formulations were found to be 53.89 ± 2.89% w/w for RPV and 53.88 ± 2.9% w/w for CAB. This enabled further work to be calculated in terms of amount of drug present, rather than simply the amount of formulation present.

FTIR analysis is shown in Fig. 6. Distinct bands in the raw drugs can be correlated back to the skeletal formulae of the compounds. The characteristic peaks in the raw RPV and CAB spectra are still seen in the spectra for their respective physical mixtures and final formulations, indicating that there have been no chemical interactions occurring during the process of formulating the NC by WBM.

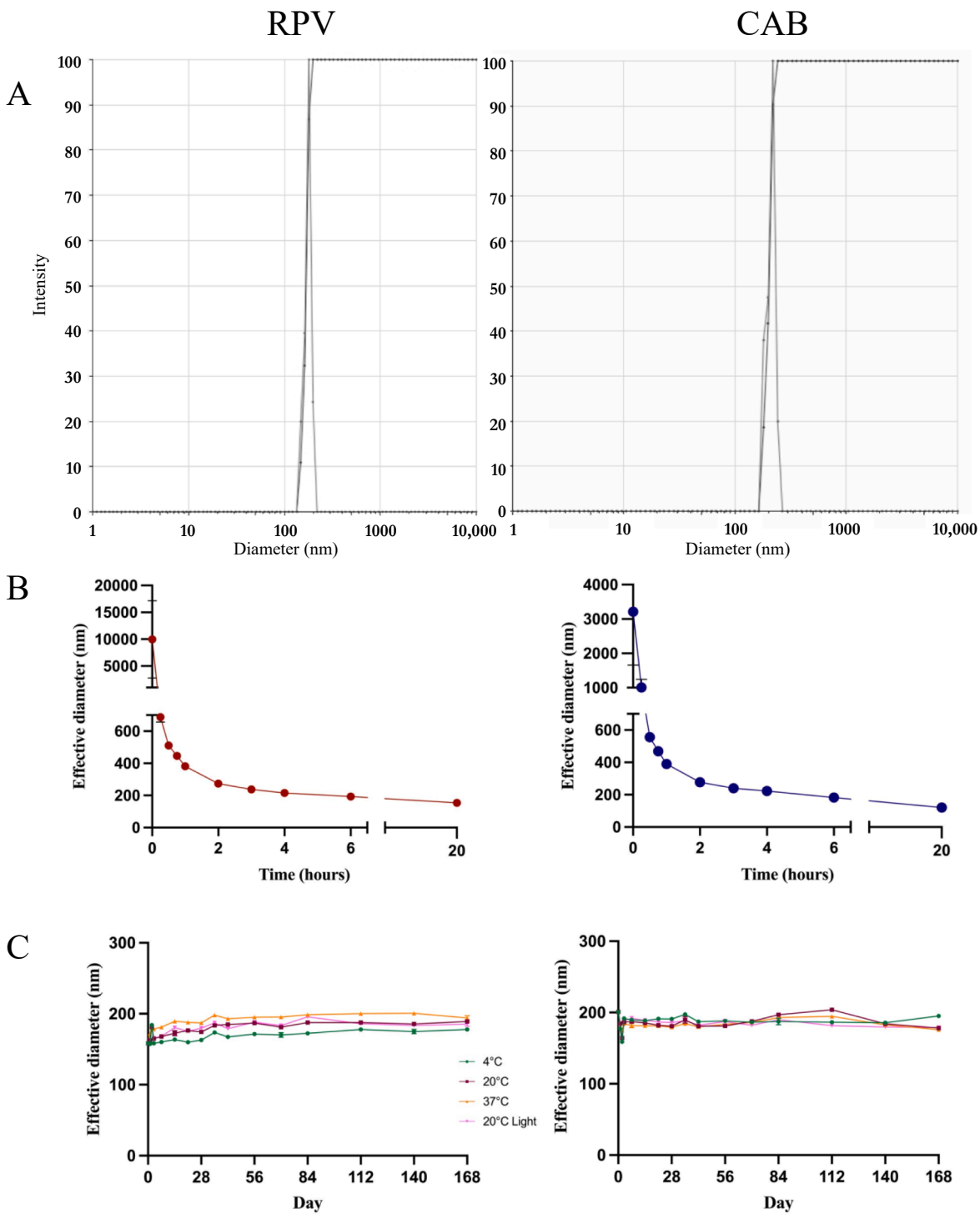

Fig. 5. The particle size and size distribution of the rilpivirine (RPV) and cabotegravir (CAB) nanocrystals (A), the particle size reduction over time in the milling process (B) and the stability of the size of the nanocrystals over a period of 6 months (C). (where applicable, means ± S.D., n = 3).

Table 3
The lyophilisation of rilpivirine (RPV) and cabotegravir (CAB) nanocrystals (NCs) with additional cryoprotectants.

Formulation	Cryoprotectanr	S_f/S_i
RPV NCs	Mannitol 5% w/v	N/A
RPV NCs	Trehalose 5% w/v	N/A
RPV NCs	Trehalose 10% w/v	206.295
RPV NCs	PVA/PVP 2%/2% 1:1	1.024
CAB NCs	PVA/PVP 2%/2% 1:1	1.020

3.5. Formulation of MN delivery systems for use in vivo

To mimic the *in vivo* for delivery into the mystacial pad using MNs, pig skin was overlaid on top of the model rat's head. Delivery is shown in Fig. 7.

The Nanosoft™ (shown in Fig. 8) were able to deliver a large quantity of drug into the skin in a 50 µl injection. This equated to a delivery efficiency of 43.78% for RPV and 58.96% for CAB, which shows an efficient system, particularly in this short window of an application

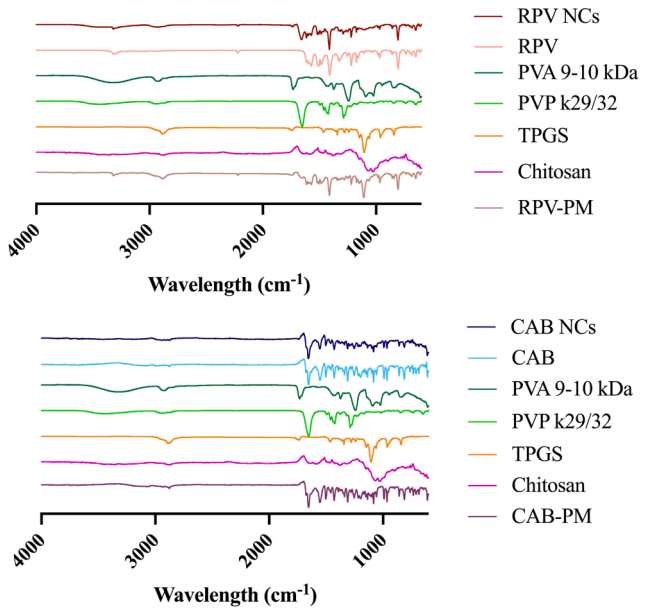

Fig. 6. Fourier transformed infrared spectroscopy for both rilpivirine (RPV) and cabotegravir (CAB) nanocrystal (NC) formulations and their individual components, as well as a physical mixture of all components.

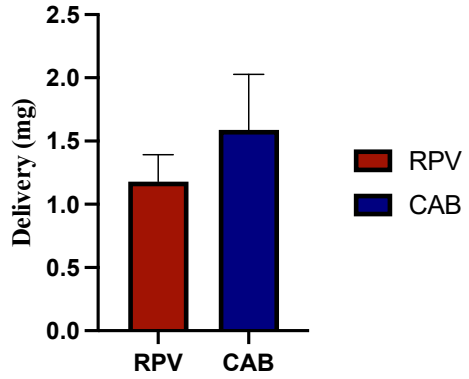

Fig. 7. Delivery of rilpivirine (RPV) and cabotegravir (CAB) from a 50 μl injection using a hollow Nanosoft™ array.

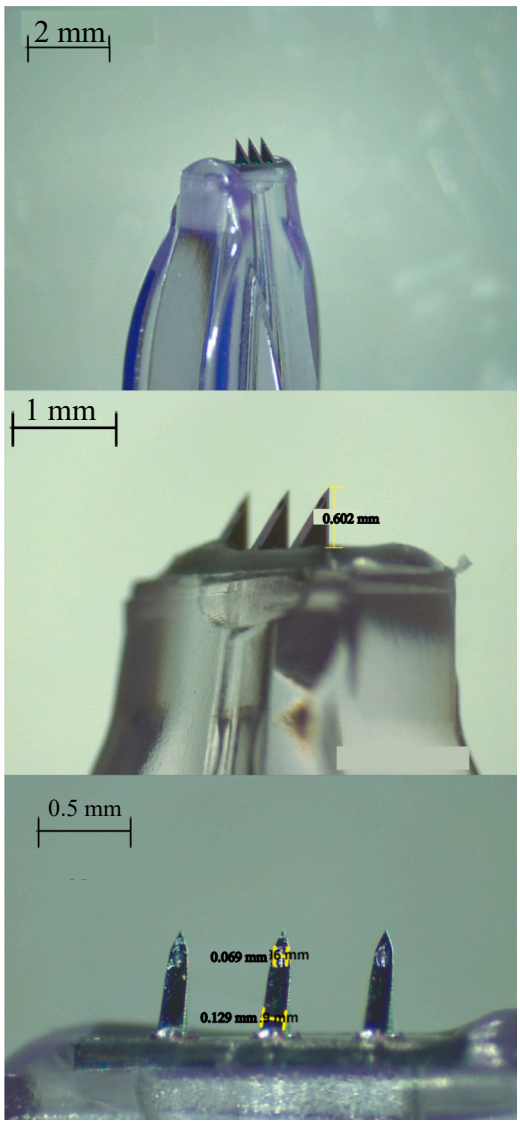

Fig. 8. Light microscope images of the Nanosoft™ hollow microneedle array used *ex vivo* and *in vivo*.

time, however, still does not approach 100%. This is partially to do with the leakage of formulation from the injection site. Steps can be taken to reduce the likelihood of this happening, such as slowing the injection rate and retracting the array slightly before deploying the plunger, but even with these steps it was not possible to achieve delivery of 100% of the formulation. This difficulty in achieving 100% efficiency with the Nanosoft™ highlights that when thinking long-term towards a product for patient use, they would not be the answer, and wouldn't be suitable for self-application, but for a challenging *in vivo* study they provide solutions to many of the problems faced.

3.6. *In vivo* MN-mediated delivery of RPV and CAB to the mystacial pad

Delivery of NCs to the mystacial pad could be visually confirmed as a white bleb in the skin, as in Fig. 9. Rats were not observed to have been in pain or discomfort following the procedure, even after analgesia had worn off. Rats were eating and drinking as normal throughout the course of the 28-day study, and as a result gained weight throughout the span of the study, as normal.

When planning the study, an oral control was decided upon as while RPV and CAB do have an IM injection marketed, many other conditions affecting the brain such as Alzheimer's disease, Parkinson's disease and schizophrenia do not have this option, and may solely have oral delivery as a treatment option. Thus, oral delivery was chosen as a control to enable translation to other potential pathologies of interest. Following this, the dose was to be considered. In previously published animal studies, rats have been administered oral RPV at doses ranging from 1 mg/kg to 25 mg/kg, and so it was known to be well tolerated (Rao et al., 2018; van 't Klooster et al., 2010; Zainuddin et al., 2017). Likewise, CAB has been seen to be delivered at 30 mg/kg and 45 mg/kg in single doses, and even up to 1000 mg/kg/day (Bowers et al., 2015; Gautam et al., 2021; Mohan et al., 2022; Pons-Faudoa et al., 2019). As these drugs are well established and tolerated as oral treatments, an approximate dose of 10 mg/kg was decided upon for both drugs, which assuming a 250 g body weight per rat would be 2.5 mg. For the MN dose, initially 50 μl of a 54 mg/ml nanosuspension was planned to be administered, which would make a 2.7 mg dose as in However, on consultation with the vet, a maximum administration volume of 25 μl was set. This was, therefore, a dose of 1.35 mg. While the oral dose was greater than the MN dose applied in this case, oral bioavailability of RPV is seen to be 32% and absorption highly dependent on fed state, while CAB absolute bioavailability hasn't been studied (Crauwels et al., 2013; European Medicines Agency, 2020a, 2011). It was thus decided to maintain the

Fig. 9. The mystacial pad area immediately after delivery of the nanocrystals using the hollow microneedle array. Circled in red is the rilpivirine delivery site on the rats right side, with the blue circle highlighting the cabotegravir injection site on the rats left side. These rats were designated to be culled at later predetermined timepoints.

oral dose at 2.5 mg for each drug, to ensure sufficient delivery for comparison.

Throughout this study, the effective doses needed for eradication of HIV in lymph and brain reservoirs have been translated from the plasma IC90 and 4IC90 values for RPV and CAB respectively (Patel et al., 2019; Tekko et al., 2022; Whitfield et al., 2016). While these values are well established for depletion of the viral load in the plasma, the levels needed to eradicate viral sanctuaries of HIV in the brain and lymph have not been covered as extensively (Asahchop et al., 2017). For example, when considering RPV, the IC90 is calculated factoring in the high plasma-protein binding of the drug. The environment in the brain is, clearly, different to that of plasma, and so there may be increased binding to different proteins present, or indeed the drug may be found more unbound and free to enact it's pharmaceutical effect (Asahchop et al., 2017; Bertrand et al., 2016). In many studies, cerebrospinal fluid (CSF) drug levels are used as a replacement for brain tissue concentrations, but this has been shown to be drug specific, and not a suitable surrogate for the brain tissue levels (Srinivas et al., 2019). If the drug levels are found to be insufficient in the brain, not only can the reservoir persist, but resistance patterns could form here readily, affecting susceptibility to treatment in both the reservoir and in the plasma (Asahchop et al., 2017; Bertrand et al., 2016). Clearly, more work is needed to determine effective doses in these compartments, but in the absence of this information, the plasma IC90 and 4IC90 are used to denote therapeutic significance for RPV and CAB, respectively.

3.6.1. *In vivo delivery of RPV*

Drug concentrations in plasma, axial lymph nodes, inguinal lymph nodes and brain were obtained using HPLC-MS. The RPV t_{max} and C_{max} are shown in Table 4.

Levels found in each tissue over the course of the 28 day study are shown in Fig. 10. To calculate the %DTE and %DTP, as shown in Table 5, mean concentrations at each timepoint were used. If values were below the LLOQ, they were assigned a value equivalent to the LOD for that matrix. If drug concentrations were below the LOD, or indeed not detectable, they were assigned a value of 1 ng/ml or 1 ng/g, as values of '0' could not be inputted into the equation.

At 24 h, oral plasma levels were below the IC90, which followed an expected pattern, due to RPV's once daily oral regimen (European Medicines Agency, 2011). With the MN delivery, low levels in plasma were expected to be seen throughout due to the nature of the study, where plasma levels were not the target of the delivery *via* the facial intradermal injection. Unlike the oral delivery, the NCs are likely to form a depot due to the reduced solubility and while *in situ* can continue to be transported to the brain over time, whereas once the oral delivery has passed through the gastrointestinal system, no further delivery will be seen. It was hypothesised that lymph delivery may be seen as a secondary targeting method, possibly by macrophage uptake at the deposition site, however this was not seen for the MN group.

Table 4
The t_{max} and C_{max} of rilpivirine in each biological matrix. (means ± S.D., n = 4 for plasma and lymph, n = 3 for brain).

Matrix	Microneedle		Oral	
	C_{max} (ng/ml, ng/g)	t_{max} (days)	C_{max} (ng/ml, ng/g)	t_{max} (days)
Plasma	17.89 ± 14.86	1	3.24 ± 3.77	3
Axillary lymph	23.50 ± 31.48	7	8.88 ± 17.75	3
Inguinal lymph	8.85 ± 16.90	3	17.11 ± 23.50	3
Brain	619.17 ± 73.32	21	478.31 ± 320.86	28

Looking at RPV content in the brain, both oral and MN delivery show brain concentrations of above the IC90. Considering oral delivery first, these levels were unexpected. While RPV is a small, hydrophobic molecule and in theory has ideal characteristics to partition through the selectively permeable BBB, it was thought that these same drug properties would result in low plasma levels, which would result in levels in the brain that were not clinically useful (Pardridge, 2012; Seelig et al., 1994). However, this study has shown an oral delivery that resulted in high levels of drug, above that of the IC90, in the brain. Based on the plasma profile plasma levels that were found, it is possible these levels did come about from absorption into the blood stream and partitioning through to the brain in the initial portion of the study. The bulk of this absorption probably occurred within the first 24 h, up until the first timepoint, and so plasma levels may have even been higher at 2 or 3 h, for example, prior to this initial sampling timepoint. Once in the plasma,

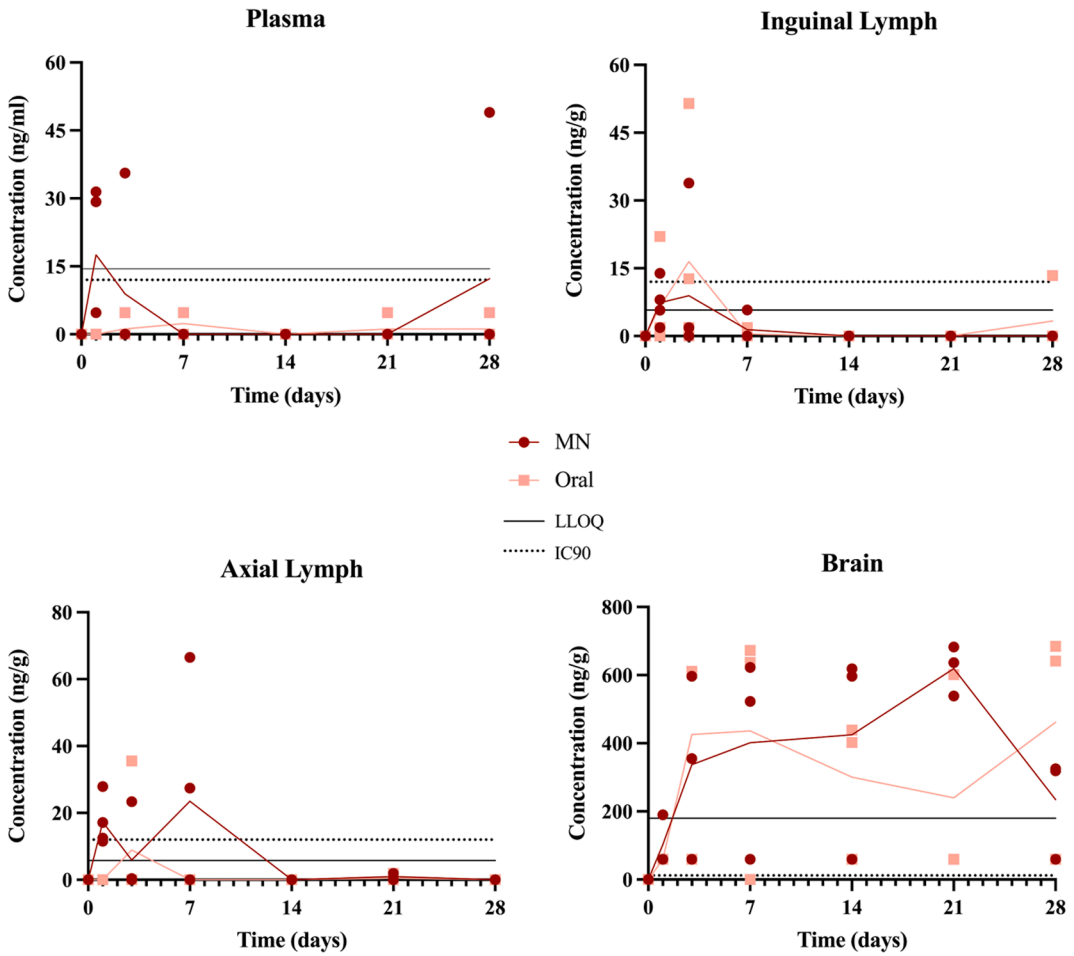

Fig. 10. The levels of rilpivirine (RPV) found in the different tissue compartments following microneedle (MN) mediated delivery and oral gavage. or using a microneedle (MN) array. The lower limit of quantification for the analytical method is displayed with a solid black line, with the dashed line representing therapeutically relevant concentrations. Plotted are the individual values, with the trendline denoting the means.

Table 5
The %DTE and %DTP for brain delivery of rilpivirine using a microneedle delivery system versus an oral control.

Timepoint (days)	%DTE	%DTP
1	16.59	−502.67
3	8.75	−1042.84
7	228.38	56.21
14	144.25	30.68
21	307.79	67.51
28	4.17	−2296.94

partitioning through the BBB into the brain resulted in the high concentrations here, above that of the IC90, and due to reduced clearance, these levels persisted throughout the course of the study. There is the potential that other transport mechanisms may have been used, which may involve macrophage delivery to the brain, however further work would be needed to confirm these transport routes (Dou et al., 2009; Zhao et al., 2011; Eleraky et al., 2020).

When considering the MN group, drug transport to the brain was likely due to transport *via* the trigeminal nerve (Formica et al., 2022; Yu et al., 2017). Drug levels were detected after 24 h, and then increased until 21 days, suggesting the hypothesis of a depot injection providing extended release was confirmed. Drug levels were maintained for 28 days above the IC90, indicating that a facial MN application could be used to deliver enough RPV to treat the viral reservoir here, and RPV has already been identified as a likely candidate to treat HAND (Ntshangase et al., 2019). Of course, the doses may need adjusted based on more information regarding effective concentrations in the brain, but even if a value of 4IC90 was used to crudely account for this, every timepoint in the MN group exceeds this. A 28 day delivery from a single MN application is potentially very patient acceptable, and could be attributed to both a depot of the NCs, and reduced clearance of the drugs once they penetrate into the brain tissue (Bertrand et al., 2016; Tekko et al., 2022; Vora et al., 2021). Cautiously, it can be hypothesised that a once monthly facial application could provide sufficient levels to combat HAND and deplete the reservoir in the brain, while RPV IM injections, or even other RPV long-acting MAPs, could be used to deliver to achieve concurrent IC90 plasma levels (Moffatt et al., 2022).

3.6.2. *In vivo delivery of CAB*

Drug concentrations in plasma, axial lymph nodes, inguinal lymph nodes and brain were obtained using HPLC-MS. The CAB t_{max} and C_{max} are shown in Table 6.

Levels found in each tissue over the course of the 28 day study are shown in Fig. 11. To calculate the %DTE and %DTP, as shown in Table 7, mean concentrations at each timepoint were used. If values were below the LLOQ, they were assigned a value equivalent to the LOD for that matrix. If drug concentrations were below the LOD, or indeed not detectable, they were assigned a value of 1 ng/ml or 1 ng/g, as values of '0' could not be inputted into the equation.

Regarding CAB, plasma levels were high, with mean levels surpassing the 4IC90 for both MN and oral delivery, for up to 28 days and 21 days respectively. Oral delivery showed levels to exceed the 4IC90, and

Table 6
The t_{max} and C_{max} of cabotegravir in each biological matrix. (means ± S.D., n = 4 for plasma and lymph, n = 3 for brain).

Matrix	Microneedle		Oral	
	C_{max} (ng/ml, ng/g)	t_{max} (days)	C_{max} (ng/ml, ng/g)	t_{max} (days)
Plasma	13579.86 ± 5284.55	1	2663.91 ± 1470.48	1
Axillary lymph	7137.95 ± 2919.71	21	694.61 ± 423.07	7
Inguinal lymph	4047.21 ± 1964.53	21	442.76 ± 143.06	1
Brain	816.38 ± 722.42	3	169.52 ± 142.01	1

after 7 days the concentrations continued to exceed this but were noticeably decreased. This initial peak, followed by a steady drop in plasma levels, again ties in with the recommended oral once daily dosing regimen (European Medicines Agency, 2020a). What was surprising, was to see the plasma levels in the MN group. The levels here, while no statistical analysis was undertaken, were much greater than those found with oral delivery. Plasma levels here also far exceeded the 4IC90, and were seen to stay above this level for 28 days. Although not the target of the study, these plasma levels were promising to see, as it shows that if a facial application was to be translated to patient use, it is possible that CAB MAPs could be administered solely to the face, without the need for concurrent oral or IM delivery. It is likely that the NCs deposited in the face have resulted in a depot effect, releasing drug into the plasma over time (Moffatt et al., 2022; Tekko et al., 2022). When compared to RPV, CAB is a more soluble drug, which does explain the increased plasma delivery, however the large extent of which and the increased length of time above the 4IC90 particularly promising for future considerations.

CAB lymph delivery was found to be similar to RPV in that in general, both sites exhibited similar patterns. With the oral delivery, while drug was detected throughout the course of the 28 day study, the 4IC90 was only exceeded at one timepoint in both sites combined throughout the course of the study. On the other hand, MN delivery showed a much greater concentration of drug in the lymph tissue at both sites, with values exceeding the 4IC90 throughout the full course of the study. These lymph node levels are likely to have come as a result of the plasma levels discussed above, with fluid draining from the blood into the lymphatic system (Hansen et al., 2015; Moore and Bertram, 2018). While this is the most likely cause of the high drug levels exceeding the 4IC90, accumulation in the lymph is possible due to the formulation of the NC. It has been shown that particles of approximately 200 nm, as for the CAB NC, have been used to specifically target the lymphatic system, and while not seen to a great extent with the RPV formulation in this

Table 7
The %DTE and %DTP for brain delivery of cabotegravir using a microneedle delivery system versus an oral control.

Timepoint (days)	%DTE	%DTP
1	34.13	−193.02
3	111.54	−10.32
7	147.13	32.03
14	4663.16	97.86
21	85.15	−17.43
28	985.67	89.53

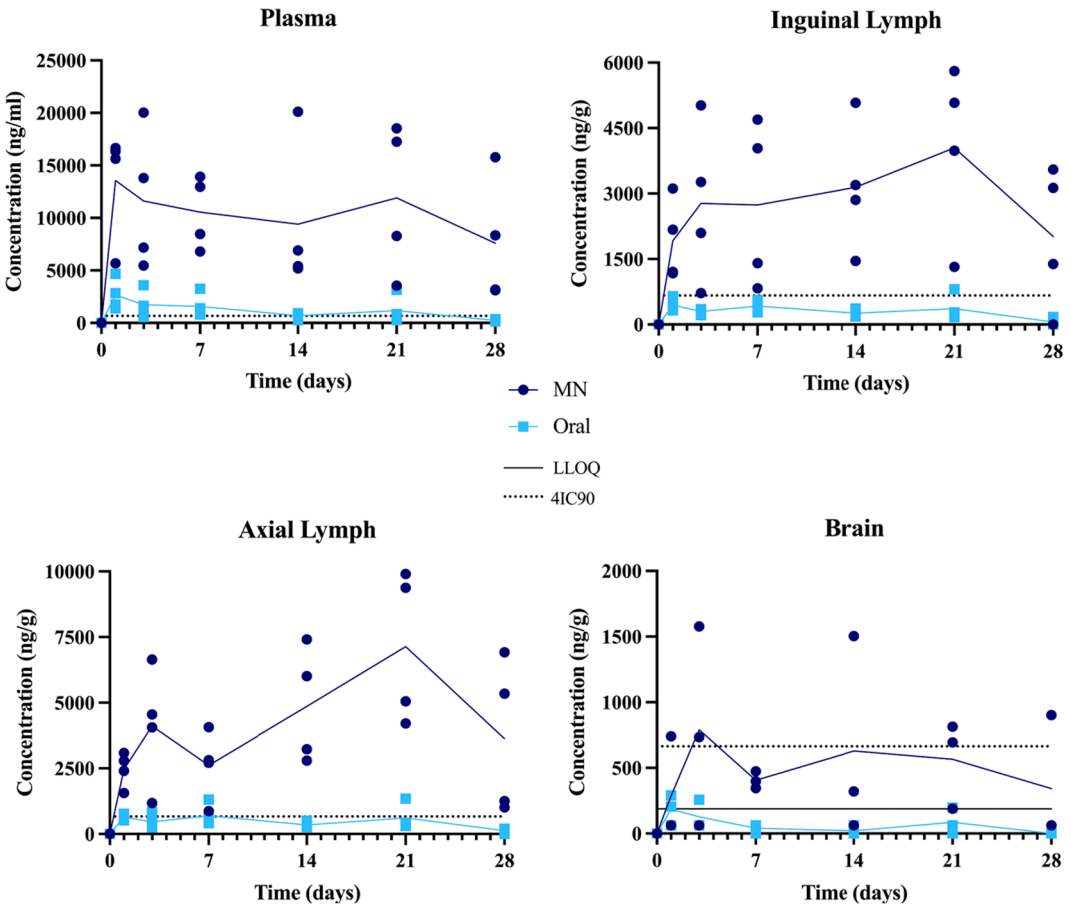

Fig. 11. The levels of cabotegravir (CAB) found in the different tissue compartments following microneedle (MN) mediated delivery and oral gavage. or using a microneedle (MN) array. The lower limit of quantification for the analytical method is displayed with a solid black line, with the dashed line representing therapeutically relevant concentrations. Plotted are the individual values, with the trendline denoting the means.

study, there is the potential this was also a mechanism for lymph delivery (De Koker et al., 2016; McCrudden et al., 2018; Videira et al., 2002). As for CAB delivery to plasma, these facial intradermal MN levels exceed the 4IC90, and could provide an option as a delivery method to target both plasma and the lymph reservoir, without the need for concurrent CAB oral or IM administration (Banga et al., 2021; Busman-Sahay et al., 2021; Wong and Yukl, 2016).

While no statistical analysis was performed due to high levels of variation, it is clear that delivery of CAB to the brain using the MN system exceeded that from the oral group. Following MN administration, an initial peak at 24 h is observed followed by a slow reduction in brain levels. The delivery of CAB to the brain could have been *via* the trigeminal route pathway as hypothesised for RPV, but has the potential to have been delivered *via* the plasma. These unexpectedly high plasma levels from the MN group, greatly exceeding the 4IC90, mean that drug may have reached the brain following partitioning through the BBB, while also bypassing it completely *via* the neural routes. While this hypothesised dual-transport mechanism did deliver more drug than the oral cohort, mean tissue levels fell short of the 4IC90 target. This is potentially due to the high variation in the samples, and if considering individual rat concentrations, many samples were above the therapeutically relevant threshold. Taking this into account, it is not unreasonable to suggest that a facial delivery of CAB NCs could result in plasma, lymph and brain concentrations that are all therapeutically relevant. The oral CAB delivery resulted in levels in the brain that were, at every timepoint, below the 4IC90. This was expected, where while CAB is extremely effective at reducing the viral load in the plasma, drugs often cannot cross the BBB in clinically useful quantities to exert their effect.

3.6.3. %DTE and %DTP of RPV and CAB

The %DTE and %DTP were calculated for both the RPV and CAB formulations. RPV showed more efficient brain delivery and targeting at 7 days, 14 days and 21 days, while the remaining timepoints were not shown to have an efficient brain delivery. These equations are computed using the unexpectedly high brain levels of RPV, above that of the IC90, following oral administration. So, while the MN system clearly delivers RPV NCs to the brain, when it is compared to the oral group which also appears to show an efficient brain delivery, %DTE and %DTP are not seen to show the efficiency of this MN system. CAB was seen to have efficient targeting and delivery at 3 days, 7 days, 14 days and 28 days, with the calculation likely skewed due to the unexpected high plasma levels following MN administration, above the 4IC90 at every timepoint measured, decreasing the 'efficiency' of the brain delivery. It is clear, however, that using this MN system, potentially therapeutically relevant plasma, lymph and brain levels were achieved, and this could be used as an option to deliver CAB to all three HIV reservoirs, and potentially combat the virus.

3.7. Future considerations

When thinking towards patient use, both the generated RPV and CAB NCs have shown their potential for combatting HAND, and indeed their potential in treating reservoirs in the blood and lymph too. As mentioned, due to the manipulation and training needed to use the hollow MN system, it is unlikely that the formulations would make it to market in the form covered in this *in vivo* study. Instead, a dissolving MAP would appear to be much more patient friendly, particularly when considering the current use of cosmetic 'face masks' on the intended application site and the well-received act of cosmetic microneedling on the face suggesting a facial application would be patient acceptable. This would enable self-application, even if the patch size would have to be increased to one which would cover a larger area of the face to achieve therpetic levels (Ripolin et al., 2017). Careful approximations can be made to calculate the exact size of a larger patch that may be necessary for use in humans. However, many assumptions would have to be made, including what dose would be necessary to achieve effective concentrations in each different tissue, and whether or not additional oral or IM dosing would be given alongside, with the facial MN system solely focussed on treatment of HAND. Such assumptions introduce uncertainty to the calculation, and while pharmacokinetic modelling has shown patch size necessary for MAPs containing RPV and CAB, this was solely considering plasma levels (Rajoli et al., 2019). Due to the uncertainly of these calculations, there would be no value in hypothesising a potential patch size, and while there is limited space available on the human face when compared to their upper arm, for example, the common use of cosmetic face masks has shown that if needed to wear a large 'mask', or large MAP, overnight, this could potentially be patient acceptable. In the future, this 'mask' could be studied further, as indeed could the impact of the morphology of each particular NC on the distribution of them in the body, and possibly their internalisation by different cells.

4. Conclusion

Formulated NCs of RPV and CAB were delivered, using a hollow MN system, to the mystacial pad area in Sprague-Dawley rats. At predetermined timepoints, plasma, lymph tissue and brain were collected and analysed *via* HPLC-MS to determine to what extent the brain was targeted, when compared to an oral control. The RPV formulation showed potentially therapeutically relevant delivery to the brain, with all rats at every timepoint, including 28 days, showing that the IC90 had been exceeded. However, delivery to lymph tissue and plasma was comparatively low. CAB showed high delivery to lymph tissue and plasma, with concentrations greatly exceeding the therapeutically relevant 4IC90 threshold. CAB delivery to the brain did also exceed that achieved with oral delivery. This study showed that, by using a patient friendly MN system, that brain delivery could be targeted using a facial intradermal delivery for the potential treatment of HAND.

Funding sources

This work was supported by Queen's University Belfast and the Department for the Economy Northern Ireland. This project was also supported in part by EPSRC grant EP/S028919/1.

CRediT authorship contribution statement

Marco T.A. Abbate: Conceptualization, Data curation, Formal analysis, Investigation, Project administration, Validation, Visualization, Writing – original draft, Writing – review & editing. **Inken K. Ramöller:** Investigation, Formal analysis, Validation. **Akmal H. Sabri:** Investigation. **Alejandro J. Paredes:** Conceptualization. **Aaron J. Hutton:** Investigation. **Peter E. McKenna:** Investigation. **Ke Peng:** Investigation. **Jessica A. Hollett:** Investigation. **Helen O. McCarthy:** Project administration, Resources. **Ryan F. Donnelly:** Conceptualization, Methodology, Resources, Writing – review & editing, Supervision, Project administration, Funding acquisition.

Declaration of Competing Interest

The authors declare the following financial interests/personal relationships which may be considered as potential competing interests: Marco Abbate reports financial support was provided by Northern Ireland Department for the Economy.

Data availability

Data will be made available on request.

References

Agrawal, M., Saraf, S., Saraf, S., Antimisiaris, S.G., Chougule, M.B., Shoyele, S.A., Alexander, A., 2018. Nose-to-brain drug delivery: An update on clinical challenges and progress towards approval of anti-Alzheimer drugs. J. Control. Release 281, 139–177. https://doi.org/10.1016/j.jconrel.2018.05.011.

Alkilani, A.Z., McCrudden, M.T.C., Donnelly, R.F., 2015. Transdermal drug delivery: Innovative pharmaceutical developments based on disruption of the barrier properties of the *stratum corneum*. Pharmaceutics 7, 438–470. https://doi.org/10.3390/PHARMACEUTICS7040438.

Asahchop, E.L., Meziane, O., Mamik, M.K., Chan, W.F., Branton, W.G., Resch, L., Gill, M. J., Haddad, E., Guimond, J.V., Wainberg, M.A., Baker, G.B., Cohen, E.A., Power, C., 2017. Reduced antiretroviral drug efficacy and concentration in HIV-infected microglia contributes to viral persistence in brain. Retrovirology 14, 1–17. https://doi.org/10.1186/S12977-017-0370-5/TABLES/2.

Banga, R., Munoz, O., Perreau, M., 2021. HIV persistence in lymph nodes. Curr. Opin. HIV AIDS 16, 209–214. https://doi.org/10.1097/COH.0000000000000686.

Bertrand, L., Nair, M., Toborek, M., 2016. Solving the blood-brain barrier challenge for the effective treatment of HIV replication in the central nervous system. Curr. Pharm. Des. 22, 5477–5486. https://doi.org/10.2174/1381612822666160726113001.

Bowers, G.D., Culp, A., Reese, M.J., Tabolt, G., Moss, L., Piscitelli, S., Huynh, P., Wagner, D., Ford, S.L., Gould, E.P., Pan, R., Lou, Y., Margolis, D.A., Spreen, W.R., 2015. Disposition and metabolism of cabotegravir: a comparison of biotransformation and excretion between different species and routes of administration in humans. Xenobiotica 46, 147–162. https://doi.org/10.3109/00498254.2015.1060372.

Bozdag, S., Dillen, K., Vandervoort, J., Ludwig, A., 2005. The effect of freeze-drying with different cryoprotectants and gamma-irradiation sterilization on the characteristics of ciprofloxacin HCl-loaded poly(D, L-lactide-glycolide) nanoparticles. J. Pharm. Pharmacol. 57, 699–707. https://doi.org/10.1211/0022357056145.

Busman-Sahay, K., Starke, C.E., Nekorchuk, M.D., Estes, J.D., 2021. Eliminating HIV reservoirs for a cure: The issue is in the tissue. Curr. Opin. HIV AIDS 16, 200–208. https://doi.org/10.1097/COH.0000000000000688.

Collnot, E.M., Baldes, C., Schaefer, U.F., Edgar, K.J., Wempe, M.F., Lehr, C.M., 2010. Vitamin E TPGS P-Glycoprotein inhibition mechanism: Influence on conformational flexibility, intracellular ATP levels, and role of time and site of access. Mol. Pharm. 7, 642–651. https://doi.org/10.1021/MP900191S.

Crauwels, H.M., Van Heeswijk, R.P.G., Buelens, A., Stevens, M., Boven, K., Hoetelmans, R.M.W., 2013. Impact of food and different meal types on the pharmacokinetics of rilpivirine. J. Clin. Pharmacol. 53, 834–840. https://doi.org/10.1002/JCPH.107.

Dalpiaz, A., Pavan, B., 2018. Nose-to-brain delivery of antiviral drugs: A way to overcome their active efflux? Pharmaceutics 10, 1–15. https://doi.org/10.3390/pharmaceutics10020039.

De Angelis, M., Schriever, S.C., Kyriakou, E., Sattler, M., Messias, A.C., Schramm, K.-W., Pfluger, P.T., 2020. Detection and quantification of the anti-obesity drug celastrol in murine liver and brain. Neurochem. Int. 136, 104713 https://doi.org/10.1016/j.neuint.2020.104713.

De Koker, S., Cui, J., Vanparijs, N., Albertazzi, L., Grooten, J., Caruso, F., De Geest, B.G., 2016. Engineering polymer hydrogel nanoparticles for lymph node-targeted delivery. Angew. Chemie 128, 1356–1361. https://doi.org/10.1002/ange.201508626.

Diamond, M.E., Arabzadeh, E., 2013. Whisker sensory system – From receptor to decision. Prog. Neurobiol. 103, 28–40. https://doi.org/10.1016/J.PNEUROBIO.2012.05.013.

Donnelly, R.F., Singh, T.R.R., Morrow, D.I.J., Woolfson, A.D. (Eds.), 2012. Microneedle-Mediated Transdermal and Intradermal Drug Delivery. Wiley.

Donnelly, R.F., McCrudden, M.T.C., Zaid Alkilani, A., Larrañeta, E., McAlister, E., Courtenay, A.J., Kearney, M.-C., Singh, T.R.R., McCarthy, H.O., Kett, V.L., Caffarel-Salvador, E., Al-Zahrani, S., Woolfson, A.D., Yamamoto, M., 2014. Hydrogel-forming microneedles prepared from "super swelling" polymers combined with lyophilised wafers for transdermal drug delivery. PLoS One 9 (10), e111547.

Eleraky, E., Omar, N.M., Mahmoud, M.A., Abou-Taleb, H.A., Nanostructured, H., 2020. Lipid Carriers to Mediate Brain Delivery of Temazepam: Design and In Vivo Study. Pharmaceutics 12, 451. https://doi.org/10.3390/pharmaceutics12050451.

Edagwa, B.J., Zhou, T., Mcmillan, J.M., Liu, X.-M., Gendelman, H.E., 2014. Development of HIV reservoir targeted long acting nanoformulated antiretroviral therapies. Curr. Med. Chem. 21, 4186–4198. https://doi.org/10.2174/0929867321666140826114135.

European Medicines Agency, 1995. ICH Q2 (R1) Validation of analytical procedures [WWW Document]. URL https://www.ema.europa.eu/en/ich-q2r2-validation-analytical-procedures (accessed 10.20.22).

European Medicines Agency, 2011. CHMP Assessment Report: Edurant.

European Medicines Agency, 2020a. CHMP Assessment Report: Vocabria.

European Medicines Agency, 2020b. CHMP Assessment Report: Rekambys.

European Medicines Agency, 2022. ICH M10 on bioanalytical method validation [WWW Document]. URL https://www.ema.europa.eu/en/ich-m10-bioanalytical-method-validation (accessed 10.20.22).

Formica, M.L., Real, D.A., Picchio, M.L., Catlin, E., Donnelly, R.F., Paredes, A.J., 2022. On a highway to the brain: A review on nose-to-brain drug delivery using nanoparticles. Appl. Mater. Today 29, 101631. https://doi.org/10.1016/J.APMT.2022.101631.

Gautam, N., McMillan, J.E.M., Kumar, D., Bade, A.N., Pan, Q., Kulkarni, T.A., Li, W., Sillman, B., Smith, N.A., Shetty, B.L.D., Szlachetka, A., Edagwa, B.J., Gendelman, H. E., Alnouti, Y., 2021. Lipophilic nanocrystal prodrug-release defines the extended pharmacokinetic profiles of a year-long cabotegravir. Nat. Commun. 12, 1–13. https://doi.org/10.1038/s41467-021-23668-x.

Gol, D., Thakkar, S., Misra, M., 2018. Nanocrystal-based drug delivery system of risperidone: lyophilization and characterization. Drug Dev. Ind. Pharm. 44, 1458–1466. https://doi.org/10.1080/03639045.2018.1460377.

Guo, Y., Luo, J., Tan, S., Otieno, B.O., Zhang, Z., 2013. The applications of Vitamin E TPGS in drug delivery. Eur. J. Pharm. Sci. 49, 175–186. https://doi.org/10.1016/j.ejps.2013.02.006.

Hanafy, A.S., Farid, R.M., Elgamal, S.S., 2015. Complexation as an approach to entrap cationic drugs into cationic nanoparticles administered intranasally for Alzheimer's disease management: Preparation and detection in rat brain. Drug Dev. Ind. Pharm. 41, 2055–2068. https://doi.org/10.3109/03639045.2015.1062897.

Hansen, K.C., D'Alessandro, A., Clement, C.C., Santambrogio, L., 2015. Lymph formation, composition and circulation: a proteomics perspective. Int. Immunol. 27, 219–227. https://doi.org/10.1093/INTIMM/DXV012.

Joint United Nations Programme on HIV/AIDS (UNAIDS), 2021. Global HIV & AIDS statistics — Fact sheet | UNAIDS [WWW Document]. 2021. URL https://www.unaids.org/en/resources/fact-sheet (accessed 2.2.22).

Kumar, S., Gokhale, R., Burgess, D.J., 2014. Sugars as bulking agents to prevent nanocrystal aggregation during spray or freeze-drying. Int. J. Pharm. 471, 303–311. https://doi.org/10.1016/J.IJPHARM.2014.05.060.

Kurakula, M., El-Helw, A.M., Sobahi, T.R., Abdelaal, M.Y., 2015. Chitosan based atorvastatin nanocrystals: Effect of cationic charge on particle size, formulation stability, and *in vivo* efficacy. Int. J. Nanomedicine 10, 321–334. https://doi.org/10.2147/IJN.S77731.

Labarthe, L., Gelé, T., Gouget, H., Benzemrane, M.S., Le Calvez, P., Legrand, N., Lambotte, O., Le Grand, R., Bourgeois, C., Barrail-Tran, A., 2022. Pharmacokinetics and tissue distribution of tenofovir, emtricitabine and dolutegravir in mice. J. Antimicrob. Chemother. 77, 1094–1101. https://doi.org/10.1093/JAC/DKAB501.

Landovitz, R.J., Li, S., Eron, J.J., Grinsztejn, B., Dawood, H., Liu, A.Y., Magnus, M., Hosseinipour, M.C., Panchia, R., Cottle, L., Chau, G., Richardson, P., Marzinke, M.A., Eshleman, S.H., Kofron, R., Adeyeye, A., Burns, D., Rinehart, A.R., Margolis, D., Cohen, M.S., McCauley, M., Hendrix, C.W., 2020. Tail-phase safety, tolerability, and pharmacokinetics of long-acting injectable cabotegravir in HIV-uninfected adults: a secondary analysis of the HPTN 077 trial. Lancet HIV 7 (7), e472–e481.

Li, J., Wang, Z., Zhang, H., Gao, J., Zheng, A., 2020. Progress in the development of stabilization strategies for nanocrystal preparations. Drug Deliv. 28, 19–36. https://doi.org/10.1080/10717544.2020.1856224.

Liu, T., Liu, X., Xiong, H., Xu, C., Yao, J., Zhu, X., Zhou, J., Yao, J., 2018. Mechanisms of TPGS and its derivatives inhibiting P-glycoprotein efflux pump and application for reversing multidrug resistance in hepatocellular carcinoma. Polym. Chem. 9, 1827–1839. https://doi.org/10.1039/C8PY00344K.

Mahajan, H.S., Mahajan, M.S., Nerkar, P.P., Agrawal, A., 2014. Nanoemulsion-based intranasal drug delivery system of saquinavir mesylate for brain targeting. Drug Deliv. 21, 148–154. https://doi.org/10.3109/10717544.2013.838014.

Masjedi, M., Azadi, A., Heidari, R., Mohammadi-Samani, S., 2020. Nose-to-brain delivery of sumatriptan-loaded nanostructured lipid carriers: preparation, optimization, characterization and pharmacokinetic evaluation. J. Pharm. Pharmacol. 72, 1341–1351. https://doi.org/10.1111/JPHP.13316.

Matsumoto, T., Takiyama, M., Sakamoto, T., Kaifuchi, N., Watanabe, J., Takahashi, Y., Setou, M., 2021. Pharmacokinetic study of Ninjin'yoeito: Absorption and brain distribution of Ninjin'yoeito ingredients in mice. J. Ethnopharmacol. 279, 114332 https://doi.org/10.1016/J.JEP.2021.114332.

McArthur, J.C., 2004. HIV dementia: An evolving disease. J. Neuroimmunol. 157, 3–10. https://doi.org/10.1016/J.JNEUROIM.2004.08.042.

McCrudden, M.T.C., Larrañeta, E., Clark, A., Jarrahian, C., Rein-Weston, A., Lachau-Durand, S., Niemeijer, N., Williams, P., Haeck, C., McCarthy, H.O., Zehrung, D., Donnelly, R.F., 2018. Design, formulation and evaluation of novel dissolving microarray patches containing a long-acting rilpivirine nanosuspension. J. Control. Release 292, 119–129. https://doi.org/10.1016/j.jconrel.2018.11.002.

McGuckin, M.B., Wang, J., Ghanma, R., Qin, N., Palma, S.D., Donnelly, R.F., Paredes, A. J., 2022. Nanocrystals as a master key to deliver hydrophobic drugs *via* multiple administration routes. J. Control. Release 345, 334–353. https://doi.org/10.1016/J.JCONREL.2022.03.012.

Mistry, A., Stolnik, S., Illum, L., 2009. Nanoparticles for direct nose-to-brain delivery of drugs. Int. J. Pharm. 379, 146–157. https://doi.org/10.1016/j.ijpharm.2009.06.019.

Moffatt, K., Tekko, I.A., Vora, L., Volpe-Zanutto, F., Hutton, A.R.J., Mistilis, J., Jarrahian, C., Akhavein, N., Weber, A.D., McCarthy, H.O., Donnelly, R.F., 2022. Development and evaluation of dissolving microarray patches for co-administered and repeated intradermal delivery of long-acting rilpivirine and cabotegravir nanosuspensions for paediatric HIV antiretroviral therapy. Pharm. Res. https://doi.org/10.1007/s11095-022-03408-6.

Mohan, H., Atkinson, K., Watson, B., Brumme, C.J., Serghides, L., 2022. A pharmacokinetic dose-optimization study of cabotegravir and bictegravir in a mouse pregnancy model. Pharmaceutics 14, 1761. https://doi.org/10.3390/PHARMACEUTICS14091761.

Moore, J.E., Bertram, C.D., 2018. Lymphatic system flows. Annu. Rev. Fluid Mech. 50 (1), 459–482.

Muntimadugu, E., Dhommati, R., Jain, A., Challa, V.G.S., Shaheen, M., Khan, W., 2016. Intranasal delivery of nanoparticle encapsulated tarenflurbil: A potential brain targeting strategy for Alzheimer's disease. Eur. J. Pharm. Sci. 92, 224–234. https://doi.org/10.1016/J.EJPS.2016.05.012.

Munyeza, C.F., Shobo, A., Baijnath, S., Bratkowska, D., Naiker, S., Bester, L.A., Singh, S. D., Maguire, G.E.M., Kruger, H.G., Naicker, T., Govender, T., 2016. Development and validation of a liquid chromatography-tandem mass spectrometry (LC-MS/MS)

method for the quantification of tigecycline in rat brain tissues. Biomed. Chromatogr. 30, 837–845. https://doi.org/10.1002/bmc.3616.
Noorulla, K.M., Yasir, M., Muzaffar, F., S, R., Ghoneim, M.M., Almurshedi, A.S., Tura, A. J., Alshehri, S., Gebissa, T., Mekit, S., Ahmed, M.M., Zafar, A., 2022. Intranasal delivery of chitosan decorated nanostructured lipid carriers of Buspirone for brain targeting: Formulation development, optimization and *in vivo* preclinical evaluation. J. Drug Deliv. Sci. Technol. 67, 102939.
Ntshangase, S., Mdanda, S., Naicker, T., Kruger, H.G., Govender, T., Baijnath, S., 2019. Rilpivirine as a potential candidate for the treatment of HIV-associated neurocognitive disorders (HAND). J. Mol. Histol. 50, 295–303. https://doi.org/10.1007/s10735-019-09826-y.
Otoki, Y., Nakagawa, K., Kato, S., Miyazawa, T., 2015. MS/MS and LC-MS/MS analysis of choline/ethanolamine plasmalogens *via* promotion of alkali metal adduct formation. J. Chromatogr. B 1004, 85–92. https://doi.org/10.1016/J.JCHROMB.2015.09.012.
Pardridge, W.M., 2012. Drug transport across the blood-brain barrier. J. Cereb. Blood Flow Metab. 32, 1959–1972. https://doi.org/10.1038/JCBFM.2012.126/ASSET/IMAGES/LARGE/10.1038_JCBFM.2012.126-FIG2.JPEG.
Patel, P., Ford, S.L., Crauwels, H., Han, K., Rossenu, S., Neyens, M., Griffith, S., Hudson, K.J., Margolis, D., Baker, M., Williams, P., Spreen, W., 2019. Pharmacokinetics of cabotegravir (CAB) and rilpivirine (RPV) long-acting (LA) injectables in HIV-infected individuals through 48 weeks in the FLAIR and ATLAS Phase 3 studies. Open Forum Infect. Dis. 6, S865. https://doi.org/10.1093/OFID/OFZ360.2173.
Pawar, V.K., Singh, Y., Meher, J.G., Gupta, S., Chourasia, M.K., 2014. Engineered nanocrystal technology: *In vivo* fate, targeting and applications in drug delivery. J. Control. Release 183, 51–66. https://doi.org/10.1016/j.jconrel.2014.03.030.
Pons-Faudoa, F.P., Sizovs, A., Di Trani, N., Paez-Mayorga, J., Bruno, G., Rhudy, J., Manohar, M., Gwenden, K., Martini, C., Chua, C.Y.X., Varchi, G., Marzinke, M.A., Grattoni, A., 2019. 2-Hydroxypropyl-β-cyclodextrin-enhanced pharmacokinetics of cabotegravir from a nanofluidic implant for HIV pre-exposure prophylaxis. J. Control. Release 306, 89–96. https://doi.org/10.1016/J.JCONREL.2019.05.037.
Rajoli, R.K.R., Flexner, C., Chiong, J., Owen, A., Donnelly, R.F., Larrañeta, E., Siccardi, M., 2019. Modelling the intradermal delivery of microneedle array patches for long-acting antiretrovirals using PBPK. Eur. J. Pharm. Biopharm. 144, 101–109. https://doi.org/10.1016/j.ejpb.2019.09.011.
Ramöller, I.K., Abbate, M.T.A., Vora, L.K., Hutton, A.R.J., Peng, K., Volpe-Zanutto, F., Tekko, I.A., Moffatt, K., Paredes, A.J., McCarthy, H.O., Donnelly, R.F., 2022. HPLC-MS method for simultaneous quantification of the antiretroviral agents rilpivirine and cabotegravir in rat plasma and tissues. J. Pharm. Biomed. Anal. 213, 114698 https://doi.org/10.1016/j.jpba.2022.114698.
Rao, M.R.P., Chaudhari, J., Trotta, F., Caldera, F., 2018. Investigation of cyclodextrin-based nanosponges for solubility and bioavailability enhancement of rilpivirine. AAPS PharmSciTech 19, 2358–2369. https://doi.org/10.1208/S12249-018-1064-6/FIGURES/10.
Reiter, B., Stimpfl, T., 2015. Quantification of drugs in brain samples. J. Anal. Toxicol. 39 (9), 702–706.
Ripolin, A., Quinn, J., Larrañeta, E., Vicente-Perez, E.M., Barry, J., Donnelly, R.F., 2017. Successful application of large microneedle patches by human volunteers. Int. J. Pharm. 521, 92–101. https://doi.org/10.1016/j.ijpharm.2017.02.011.
Rojekar, S., Vora, L.K., Tekko, I.A., Volpe-Zanutto, F., McCarthy, H.O., Vavia, P.R., Ryan, R.F., 2021. Etravirine-loaded dissolving microneedle arrays for long-acting delivery. Eur. J. Pharm. Biopharm. 165, 41–51. https://doi.org/10.1016/J.EJPB.2021.04.024.
Romero, G.B., Keck, C.M., Müller, R.H., 2016a. Simple low-cost miniaturization approach for pharmaceutical nanocrystals production. Int. J. Pharm. 501, 236–244. https://doi.org/10.1016/j.ijpharm.2015.11.047.
Romero, G.B., Keck, C.M., Müller, R.H., Bou-Chacra, N.A., 2016b. Development of cationic nanocrystals for ocular delivery. Eur. J. Pharm. Biopharm. 107, 215–222.
Sanford, M., 2012. Rilpivirine: Rilpivirine. Drugs 72 (4), 525–541.
Scherrer, Alexandra U, Traytel, A., Braun, Dominique L, Calmy, Alexandra, Battegay, Manuel, Cavassini, Matthias, Furrer, Hansjakob, Schmid, Patrick, Bernasconi, Enos, Stoeckle, M., Kahlert, C., Trkola, Alexandra, Kouyos, Roger D, Tarr, Philip, Marzolini, Catia, Wandeler, Gilles, Fellay, Jacques, Bucher, H., Yerly, Sabine, Suter, F., Hirsch, H., Huber, Michael, Dollenmaier, Günter, Perreau, Matthieu, Martinetti, Gladys, Rauch, Andri, Günthard, Huldrych F, (SHCS), the S.H.C.S., Aebi-Popp, K., Anagnostopoulos, A., Battegay, M, Bernasconi, E, Böni, J., Braun, D L, Bucher, H.C., Calmy, A, Cavassini, M, Ciuffi, A., Dollenmaier, G, Egger, M., Elzi, L., Fehr, J., Fellay, J, Furrer, H, Fux, C.A., Günthard, H F, Haerry, D., Hasse, B., Hirsch, H.H., Hoffmann, M., Hösli, I., Huber, M, Kahlert, C.R., Kaiser, L., Keiser, O., Klimkait, T., Kouyos, R D, Kovari, H., Ledergerber, B., Martinetti, G, Martinez de Tejada, B., Marzolini, C, Metzner, K.J., Müller, N., Nicca, D., Paioni, P., Pantaleo, G., Perreau, M, Rauch, A, Rudin, C., Scherrer, A U, Schmid, P, Speck, R., Stöckle, M., Tarr, P, Trkola, A, Vernazza, P., Wandeler, G, Weber, R., Yerly, S, 2022. Cohort profile update: The Swiss HIV Cohort Study (SHCS). Int. J. Epidemiol. 51, 33-34j. https://doi.org/10.1093/IJE/DYAB141.
Scholz, E.M.B., Kashuba, A.D.M., 2021. The lymph node reservoir: Physiology, HIV infection, and antiretroviral therapy. Clin. Pharmacol. Ther. 109, 918–927. https://doi.org/10.1002/CPT.2186.
Seelig, A., Gottschlich, R., Devant, R.M., 1994. A method to determine the ability of drugs to diffuse through the blood-brain barrier. Proc. Natl. Acad. Sci. 91, 68–72. https://doi.org/10.1073/PNAS.91.1.68.
Selvaraj, K., Gowthamarajan, K., Karri, V.V.S.R., 2018. Nose to brain transport pathways an overview: potential of nanostructured lipid carriers in nose to brain targeting. Artif. Cells, Nanomedicine Biotechnol. 46, 2088–2095. https://doi.org/10.1080/21691401.2017.1420073.
Singh, T.R.R., Tekko, I.A., Al-Shammari, F., Ali, A.A., McCarthy, H., Donnelly, R.F., 2016. Rapidly dissolving polymeric microneedles for minimally invasive intraocular drug delivery. Drug Deliv. Transl. Res. 6, 800–815. https://doi.org/10.1007/S13346-016-0332-9/FIGURES/12.
Srinivas, N., Rosen, E.P., Gilliland, W.M., Kovarova, M., Remling-Mulder, L., De La Cruz, G., White, N., Adamson, L., Schauer, A.P., Sykes, C., Luciw, P., Garcia, J.V., Akkina, R., Kashuba, A.D.M., 2019. Antiretroviral concentrations and surrogate measures of efficacy in the brain tissue and CSF of preclinical species. Xenobiotica 49, 1192–1201. https://doi.org/10.1080/00498254.2018.1539278/SUPPL_FILE/IXEN_A_1539278_SM2419.PDF.
Tekko, I.A., Permana, A.D., Vora, L., Hatahet, T., McCarthy, H.O., Donnelly, R.F., 2020. Localised and sustained intradermal delivery of methotrexate using nanocrystal-loaded microneedle arrays: Potential for enhanced treatment of psoriasis. Eur. J. Pharm. Sci. 152, 105469 https://doi.org/10.1016/j.ejps.2020.105469.
Tekko, I.A., Vora, L.K., Volpe-Zanutto, F., Moffatt, K., Jarrahian, C., McCarthy, H.O., Donnelly, R.F., 2022. Novel bilayer microarray patch-assisted long-acting micro-depot cabotegravir intradermal delivery for HIV pre-exposure prophylaxis. Adv. Funct. Mater. 32, 2106999. https://doi.org/10.1002/ADFM.202106999.
Tuan-Mahmood, T.M., McCrudden, M.T.C., Torrisi, B.M., McAlister, E., Garland, M.J., Singh, T.R.R., Donnelly, R.F., 2013. Microneedles for intradermal and transdermal drug delivery. Eur. J. Pharm. Sci. 50, 623–637. https://doi.org/10.1016/j.ejps.2013.05.005.
van 't Klooster, G., Hoeben, E., Borghys, H., Looszova, A., Bouche, M.-P., van Velsen, F., Baert, L., 2010. Pharmacokinetics and disposition of rilpivirine (TMC278) nanosuspension as a long-acting injectable antiretroviral formulation. Antimicrob. Agents Chemother. 54 (5), 2042–2050.
Verma, S., Kumar, S., Gokhale, R., Burgess, D.J., 2011. Physical stability of nanosuspensions: Investigation of the role of stabilizers on Ostwald ripening. Int. J. Pharm. 406, 145–152. https://doi.org/10.1016/j.ijpharm.2010.12.027.
Videira, M.A., Botelho, M.F., Santos, A.C., Gouveia, L.F., Pedroso de Lima, J.J., Almeida, A.J., 2002. Lymphatic uptake of pulmonary delivered radiolabelled solid lipid nanoparticles. J. Drug Target. 10, 607–613. https://doi.org/10.1080/1061186021000054933.
Volpe-Zanutto, F., Ferreira, L.T., Permana, A.D., Kirkby, M., Paredes, A.J., Vora, L.K., P. Bonfanti, A., Charlie-Silva, I., Raposo, C., Figueiredo, M.C., Sousa, I.M.O., Brisibe, A., Costa, F.T.M., Donnelly, R.F., Foglio, M.A., 2021. Artemether and lumefantrine dissolving microneedle patches with improved pharmacokinetic performance and antimalarial efficacy in mice infected with Plasmodium yoelii. J. Control. Release 333, 298–315.
Volpe-Zanutto, F., Vora, L.K., Tekko, I.A., McKenna, P.E., Permana, A.D., Sabri, A.H., Anjani, Q.K., McCarthy, H.O., Paredes, A.J., Donnelly, R.F., 2022. Hydrogel-forming microarray patches with cyclodextrin drug reservoirs for long-acting delivery of poorly soluble cabotegravir sodium for HIV Pre-Exposure Prophylaxis. J. Control. Release 348, 771–785. https://doi.org/10.1016/j.jconrel.2022.06.028.
Vora, L.K., Moffatt, K., Tekko, I.A., Paredes, A.J., Volpe-Zanutto, F., Mishra, D., Peng, K., Singh, T.R.R., Donnelly, R.F., 2021. Microneedle array systems for long-acting drug delivery. Eur. J. Pharm. Biopharm. 159, 44–76. https://doi.org/10.1016/J.EJPB.2020.12.006.
Whitfield, T., Torkington, A., van Halsema, C., 2016. Profile of cabotegravir and its potential in the treatment and prevention of HIV-1 infection: Evidence to date. HIV/AIDS - Res. Palliat. Care 8, 157–164. https://doi.org/10.2147/HIV.S97920.
Williams, P.E., Crauwels, H.M., Basstanie, E.D., 2015. Formulation and pharmacology of long-acting rilpivirine. Curr. Opin. HIV AIDS 10, 233–238. https://doi.org/10.1097/COH.0000000000000164.
Wong, J.K., Yukl, S.A., 2016. Tissue reservoirs of HIV. Curr. Opin. HIV AIDS 11, 362–370. https://doi.org/10.1097/COH.0000000000000293.
Yang, W., Han, Y.-H., Wang, H.-C., Lu, C.-T., Yu, X.-C., Zhao, Y.-Z., 2022. Intradermal injection of icariin-HP-β-cyclodextrin improved traumatic brain injury *via* the trigeminal epineurium-brain dura pathway. J. Drug Target. 30, 557–566. https://doi.org/10.1080/1061186X.2021.2023159.
Yang, C., Wu, T., Qi, Y., Zhang, Z., 2018. Recent advances in the application of Vitamin E TPGS for drug delivery. Theranostics 8, 464–485. https://doi.org/10.7150/thno.22711.
Yu, X.C., Yang, J.J., Jin, B.H., Xu, H.L., Zhang, H.Y., Xiao, J., Lu, C.T., Zhao, Y.Z., Yang, W., 2017. A strategy for bypassing the blood-brain barrier: Facial intradermal brain-targeted delivery *via* the trigeminal nerve. J. Control. Release 258, 22–33. https://doi.org/10.1016/j.jconrel.2017.05.001.
Zainuddin, R., Zaheer, Z., Sangshetti, J.N., Momin, M., 2017. Enhancement of oral bioavailability of anti-HIV drug rilpivirine HCl through nanosponge formulation. Drug Dev. Ind. Pharm. 43, 2076–2084. https://doi.org/10.1080/03639045.2017.1371732.
Zayyad, Z., Spudich, S., 2015. Neuropathogenesis of HIV: From initial neuroinvasion to HIV-associated neurocognitive disorder (HAND). Curr. HIV/AIDS Rep. 12, 16–24. https://doi.org/10.1007/s11904-014-0255-3.